

# Calibrating the *Swift*/UVOT to Standard Optical Photometry with Observations of Landolt Standards and Supernova 2005am

Weidong Li, Saurabh Jha, Alexei V. Filippenko, Joshua S. Bloom, David Pooley, Ryan J.  
Foley, & Daniel A. Perley

Department of Astronomy, University of California, Berkeley, CA 94720-3411.

email: (wli,sjha,alex,jbloom,dave,rfoley,dperley)@astro.berkeley.edu

Received \_\_\_\_\_; accepted \_\_\_\_\_

Submitted to PASP

## ABSTRACT

The Ultraviolet-Optical Telescope (UVOT) onboard *Swift* has the capability to provide critical insight into the physics of the early afterglows of gamma-ray bursts (GRBs). But without precise calibration of the UVOT to standard photometric systems, it is impossible to leverage late-time, ground-based follow-up data to the early-time UVOT observations. In this paper we present an empirical determination of the photometric zero points and the optimal photometric parameters to analyze  $U$ -,  $B$ -, and  $V$ -band images obtained with *Swift*/UVOT. We base our analysis on aperture photometry performed on the local standard stars in the field of Supernova (SN) 2005am, of which UVOT has a series of images and we have ground-based calibrations and follow-up observations. We achieve a consistency of about 0.05 mag between the UVOT photometry and our ground-based calibration when the photometry aperture radius is small (2''.5 for unbinned data, 3''.0 for  $2 \times 2$  binned data), and when a correction factor is applied to the measured instrumental magnitudes. Our results are verified by reductions of a series of UVOT  $V$ -band observations of Landolt standard stars. From this analysis, preliminary photometric corrections caused by the coincidence loss for bright stars are estimated. A step-by-step photometry procedure is also presented. We analyze the UVOT  $UBV$  photometry of SN 2005am, and find that the UVOT photometry is generally consistent with the ground-based observations, but a difference of up to 0.5 mag is found when the SN became faint.

We discuss the limitations of our photometric calibrations, the possible causes of the correction factor, the scatter in the UVOT photometry, and the color terms of the UVOT  $B$  and  $V$  filters. There is an intrinsic scatter of  $\sim 0.04$ – $0.06$  mag in our final UVOT photometry that cannot be easily accounted for and removed. To further improve the UVOT photometric precision, either the cause of this scatter must be found and fixed, or photometric procedures more sophisticated than simple aperture photometry need to be developed.

*Subject headings:* gamma-rays: bursts – space vehicles: instruments – ultraviolet: general – techniques: photometric

## 1. Introduction

The successful launch and operation of *Swift* heralds a new era for the study of gamma-ray bursts (GRBs) and related phenomena. *Swift*, a multi-wavelength space observatory, has three instruments: the Burst Alert Telescope (BAT), the X-ray Telescope (XRT), and the UV/Optical Telescope (UVOT). Together these instruments observe GRBs and their afterglows in the gamma-ray, X-ray, and ultraviolet/optical wavebands, respectively. Compared to previous space missions dedicated to the study of GRBs, the UVOT is unique to *Swift*, although it is identical to the Optical Monitor on *XMM-Newton* (Mason et al. 2001). The UVOT is a 30 cm Ritchey-Chrétien reflector, using micro-channel intensified CCDs as detectors. These are photon-counting devices capable of detecting very low signal levels. The UVOT is designed to rapidly respond to localizations of GRBs by the BAT and XRT instruments. It has UV capability which is not possible from the ground, and it is also more sensitive than most ground-based rapid-response telescopes. From the UVOT images, optical afterglows of GRBs can be quickly identified and studied, which helps to optimize ground-based observations, and provides information on the early-time photometric evolution of these GRB afterglows.

It is expected that the early UVOT observations will be used in conjunction with subsequent ground-based images. It is thus essential that the UVOT and the ground-based images are calibrated on the same photometric system. In the optical bands, the most frequently used ground-based photometric system is the Johnson/Cousins *UBVRI* system, and the *Swift* calibration database (CALDB) webpage (<http://heasarc.gsfc.nasa.gov/docs/heasarc/caldb/swift>) provides calibration files for the various UVOT filters. Table 1 lists these calibration results from the latest release (2005 Apr. 6).

Since it is important to tie the UVOT photometry with that obtained from the ground, in this paper we present an independent study of the photometric calibrations for the UVOT filters, mostly in the *B* and *V* bands, but some preliminary results are presented for the *U* band as well. This calibration is derived from observations of Supernova (SN)

2005am, for which the UVOT has multiple-epoch observations in the various filters, and for which we have excellent ground-based follow-up observations and calibrations. We have also analyzed available Landolt (1992) standard-star observations in the *Swift* quicklook database. The other goal of this paper is to analyze the UVOT observations with tools that are familiar to optical astronomers, such as IRAF and DoPhot, and search for optimal parameters for doing proper photometry. The NASA High Energy Astrophysics Science Archive Research Center (HEASARC)<sup>1</sup> has supplied software tools to analyze data from all *Swift* instruments. For UVOT images, these tools suggest aperture photometry using SExtractor (Bertin & Arnouts 1996).

The ground-based observations and reduction of SN 2005am are described in §2, and photometric calibration analyses are presented in §3. Section §4 discusses the UVOT photometry of SN 2005am and compares this to the ground-based observations. The discussion is presented in §5 and the conclusions are summarized in §6.

## 2. Analysis of the Ground-based Observations of SN 2005am

SN 2005am was discovered by R. Martin (Martin, Yamaoka, & Itagaki 2005) on 2005 Feb. 22 (UT dates are used throughout this paper) during the course of the Perth Automated SN Search. It was classified as a Type Ia SN (SN Ia) by Modjaz et al. (2005) from a spectrum taken with the F. L. Whipple Observatory 1.5-m telescope. After some delays caused by bad weather, we began to follow the SN with the robotic 0.76-m Katzman Automatic Imaging Telescope (KAIT; see Li et al. 2000; Filippenko et al. 2001; Filippenko 2003) at Lick Observatory on Mar. 6. Several epochs of observations were also obtained with the 1-m Nickel telescope at Lick Observatory.

Photometric calibrations of the SN 2005am field were performed under photometric conditions on 4 nights: Mar. 9 and 13 with KAIT, and Mar. 12 and 14 with the Nickel telescope. During each photometric night, many Landolt (1992) standard-star sequences

---

<sup>1</sup><http://heasarc.gsfc.nasa.gov/> .

(9-12 for Nickel, 16-18 for KAIT) were observed at a range of airmasses. Instrumental magnitudes for the standard stars were measured using aperture photometry with the IRAF<sup>2</sup> DAOPHOT package (Stetson 1987) and then employed to determine transformation coefficients to the standard Johnson-Cousins *BVRI* system. The derived transformation coefficients and color terms were then used to calibrate a sequence of local standard stars in the field of SN 2005am (hereafter SN 2005am stars). Figure 1 shows a finder chart for the SN 2005am field, while Table 2 lists the magnitudes of the local standard stars and the associated uncertainties derived by averaging over the photometric nights. Notice that the local standard stars have different numbers of calibrations because the two telescopes have different total fields of view. The majority of the calibrated magnitudes have uncertainties smaller than 0.03 mag.

Also listed in Table 2 are preliminary *U*-band calibrations for some of the bright stars in the SN 2005am field. This calibration was done on Apr. 6 under photometric conditions with KAIT, but only one *UBVRI* sequence of the Landolt field “Rubin 152” was observed at the same airmass as when SN 2005am was imaged. Inspection of the data also reveals that the measured *BVRI* magnitudes for the SN 2005am stars from this particular night are offset from the calibration listed in Table 2 by a constant  $0.20 \pm 0.01$  mag. Further investigation suggests that the dome was slightly blocking the telescope when the standard-star field was imaged due to a dome position zero-point error. We thus shifted the calibrated *U*-band magnitudes by the same amount. We set an uncertainty of 0.05 mag to the calibrated *U*-band magnitudes, but because we had only one standard-star sequence, and we had to apply an arbitrary shift to the measured magnitudes, the real uncertainty could be as high as 0.10 mag. As a result, we caution that all the results derived for the *U* band in this paper should be regarded as preliminary.

As can be seen in Figure 1, SN 2005am occurred in the outskirts of its host galaxy,

---

<sup>2</sup>IRAF (Image Reduction and Analysis Facility) is distributed by the National Optical Astronomy Observatories, which are operated by the Association of Universities for Research in Astronomy, Inc., under cooperative agreement with the National Science Foundation.

and is separated from a relatively bright foreground star by only 7''. To derive proper photometry for SN 2005am, we use the point-spread-function (PSF) fitting method (Stetson 1987) in the IRAF/DAOPHOT package to perform differential photometry of SN 2005am relative to the local standard stars; see Li et al. (2003) for more details. Color terms for the KAIT and the Nickel filters have been well established from photometric calibrations of over 20 photometric nights at each telescope, and have been applied to derive the final photometry for SN 2005am as listed in Table 3. The quoted uncertainty of the magnitudes is a quadrature of the PSF-fitting photometry and the transformation scatter from the local standard stars. Although SN 2005am has a complex background, the final photometry has an overall uncertainty of only 0.03–0.04 mag because the SN is significantly brighter than the background, and there are plenty of bright isolated stars in the field from which to construct a robust PSF for the images.

The derived light curve of SN 2005am is shown in Figure 2, together with fits using the Multicolor Light Curve Shape (MLCS2k2) method (Jha 2002; Jha, Riess, & Kirshner 2005b), which is an empirical method to model the light curves of a SN Ia to derive its luminosity distance. Overall, the KAIT and the Nickel photometry are consistent with each other (except perhaps the two *I*-band data points near JD 2453470). SN 2005am shows a photometric evolution rather typical of a SN Ia: a second peak in the *I* band, a shoulder in the *R* band, and a smooth decline after maximum in the bluer bands. Our follow-up observations began near the maximum of the *B* band, and 2–3 days before maximum in the other bands. The MLCS2k2 fits are typical for a well-observed SN Ia. SN 2005am is not significantly reddened by dust in its host galaxy (host  $A_V = 0.09 \pm 0.07$  mag). It is also a somewhat rapidly declining and subluminous object (by approximately 0.5 mag), intermediate between normal SNe Ia and the most subluminous objects like SN 1991bg (Filippenko et al. 1992). This makes SN 2005am an important addition to the sample of nearby SNe Ia, with only a handful of similar objects known (Jha et al. 2005a).

The SN 2005am stars as listed in Table 2 are used to study the photometric calibrations of the UVOT filters in §3. We investigate the optimal parameters to do photometry on these stars in the UVOT images, so that the best possible consistency between the

ground-based KAIT and Nickel calibrations (hereafter the “Lick calibration”) and the UVOT measurements can be achieved. These stars cover a wide range of brightness (from  $B = 12.30$  to  $B = 19.03$  mag) and color [from  $(B - V) = 0.51$  to  $(B - V) = 1.39$  mag]. The photometry of SN 2005am itself will provide ground-based estimates for the magnitudes of SN 2005am at the epochs of the UVOT observations, as discussed in §4.

### 3. Photometric Calibration of the UVOT

#### 3.1. UVOT Observations of SN 2005am

A journal of UVOT observations of SN 2005am is listed in Table 4. These are the data available to the general users after *Swift* went public on 2005 Apr. 1. We first retrieved the data from the *Swift* quicklook database, and in all cases, the level 2 filter sky images were downloaded. From the *Swift* manual, the level 2 data are what most researchers will use to start their analysis. The UVOT reduction pipeline has been performed on these images, which are also stored in sky coordinates ( $RA_{J2000}$  and  $DEC_{J2000}$ ). The accompanying exposure maps for each individual image were also downloaded. There are UVOT observations on SN 2005am in other filters ( $UVW1$ ,  $UVW2$ , and  $UVM2$ ) as well, but these images are not listed in Table 4, and will not be studied in this paper since these filters are in the far-UV where we do not have ground-based calibrations.

There are five  $UBV$  sequences observed by UVOT in Table 4, which we hereafter refer to as obs1, obs2, obs3, obs4, and obs5, respectively. The  $U$ -band observation in sequence obs1 will be referred as “obs1  $U$ ,” etc. There are only a short (18.02 s)  $U$ -band exposure, and a normal  $V$ -band exposure, in obs4; the  $B$  band is missing. All sequences were observed without binning except obs2, in which a  $2 \times 2$  on-board binning was used. The SN was well detected in all images except obs4  $U$  and obs5, for which the exposure times were too short for the brightness of the SN. The unbinned UVOT data have a resolution of  $0.5''$  per pixel, and the total field of view is  $16''.4 \times 16''.4$ . Since the fields of view of KAIT ( $6''.6 \times 6''.6$ ) and the Nickel telescope ( $6''.3 \times 6''.3$ ) are much smaller, the field for which we have ground-based calibration is only a fraction of the total UVOT field.

Inspection of the UVOT images reveals two things worth noting for observers familiar with the reduction of ground-based CCD observations. First, as shown in Figure 3 and also indicated in the *Swift* manuals, the PSFs of the stars vary with the count rate (i.e., magnitude) of the object and with the filter being used, and they may vary with position on the detector. The brightest stars also show various degrees of “ghost” emission, including ghost wings, ghost rings, and rings around the stars themselves. This is very different from ground-based CCD images, in which stars of different brightness have a constant PSF across the image (except for image distortion in wide-field images, optical defects, or stars that are saturated). As discussed more in later sections, a varying PSF is a serious challenge for doing stellar photometry, unless the intrinsic PSFs can be constructed according to the brightness of the stars and their positions on the detector. Unfortunately, the information on the intrinsic PSF was not available at the time when we conducted this study.

Another aspect of the UVOT images that is different from ground-based CCD observations is the sky background distribution and the associated noise pattern. Figure 4 shows the histograms of the sky background distribution around star #5 in the first four *U*-band observations. The histogram in obs5 *U* is not shown, but it is similar to that of obs3 *U*. These background values are extracted from an annular region with an inner radius of 35 pixels and an outer radius of 45 pixels around star #5 for unbinned data, and an inner radius of 17.5 pixels and an outer radius of 22.5 pixels for the  $2 \times 2$  binned obs2, as discussed more in the next section. As shown in the figure, only in obs2 does the sky background around star #5 show a Gaussian distribution. In the other three observations, due to the low background, the histogram peaks and truncates at background value 0, and shows a Poissonian rather than a Gaussian distribution. This is different from ground-based CCD observations in which the background distribution closely follows photon statistics and is mostly Gaussian. How to optimally account for the background contamination at the location of stars has direct impact on the photometry, as discussed more in the next section.

### 3.2. Aperture Photometry Parameters

In this paper we use  $U$ ,  $B$ , and  $V$  as the magnitudes in the standard Johnson/Cousins  $UBVRI$  system, such as the calibrated magnitudes for the local standard stars listed in Table 2. We use  $u$ ,  $b$ , and  $v$  as the instrumental magnitudes measured from the UVOT image, and  $u'(ZP)$ ,  $b'(ZP)$ , and  $v'(ZP)$  as the magnitudes measured from the photometry program with a zero point of ZP. In general,  $u = u'(ZP)$ ,  $b = b'(ZP)$ , and  $v = v'(ZP)$ , but our study requires these magnitudes to be distinguished, as discussed later in §3.2.4.

We use the “phot” task in the IRAF/DAOPHOT package to carry out the aperture photometry through out the paper. The parameters derived in our paper should be easily adaptable to other photometry programs that work on FITS images.

In theory, if one can properly estimate the sky background and use a very large aperture to sum all the flux, a varying PSF should not be a problem for doing photometry. In practice, however, a big aperture includes more sky background and its associated noise. The signal to noise ratio (S/N) for the photometry will thus diminish, so large apertures only work for bright objects. Moreover, because of contamination from neighboring objects, it is often not possible to use large sky regions or apertures when doing photometry.

For the reductions used throughout this paper, we adopted an annular sky background region with an inner radius of 35 pixels and an outer radius of 45 pixels centered on each object for unbinned data, and an inner radius of 17.5 pixels and an outer radius of 22.5 pixels for  $2 \times 2$  binned data. The full width at half maximum (FWHM) of the UVOT images is about 4.0 pixels (2.5 pixels for the  $2 \times 2$  binned data), so the sky region starts more than  $(7\text{--}8) \times \text{FWHM}$  from the source, which is further than one generally uses for ground-based photometry  $[(4\text{--}5) \times \text{FWHM}]$ . We thus expect the contamination from the source itself to the background to be small, though bigger sky regions are tested later in the paper. For bright objects that have ghost emissions as shown in Figure 3, there is considerable emission from the source itself in our defined sky region, and we will attempt to evaluate how our analyses can be applied to bright objects in §3.2.5. Fortunately, for all the local standard stars in the field of SN 2005am, only star #6 is bright and shows

a surrounding ring in most of the images. We thus exclude star #6 in our studies in the following sections, but include it in the studies for bright objects in § 3.2.5.

Another related issue when comparing the photometry from UVOT to the Lick calibration is the color terms for the UVOT  $UBV$  filters. The instrumental magnitudes from the UVOT images need to be corrected for the color terms so the UVOT photometry and the Lick calibration are in the same photometric system. Since we do not have enough calibrated stars to derive the color terms for the UVOT filters from the observations of SN 2005am, we adopt color terms from the *Swift* CALDB database. The color terms for the UVOT  $U$ ,  $B$ , and  $V$  filters as listed in the latest calibration data release (2005 Apr. 6) are as follows:

$$U - B = 0.0347 + 0.8484(u - b) + 0.0649(u - b)^2, \quad (1)$$

$$U - V = 0.087 + 0.8926(u - v) + 0.0274(u - v)^2, \quad (2)$$

$$B - V = 0.0148 + 1.0184(b - v), \quad (3)$$

$$B = b + 0.0173 + 0.0187(u - b) + 0.013(u - b)^2 - 0.0108(u - b)^3 - 0.0058(u - b)^4 + 0.0026(u - b)^5, \text{ and} \quad (4)$$

$$V = v + 0.0006 - 0.0113(b - v) + 0.0097(b - v)^2 - 0.0036(b - v)^3. \quad (5)$$

The uncertainties of the coefficients have not been reported. These equations are only valid for the range of colors  $-1.468 < (U - B) < 1.804$  mag,  $-1.852 < (U - V) < 3.306$  mag, and  $-0.384 < (B - V) < 1.642$  mag.

For the color ranges in which these equations are valid, the difference between  $B$  and  $b$  (Eq. 4), and  $V$  and  $v$  (Eq. 5) is  $< 0.02$  mag, significantly smaller than the photometric precision that we can achieve in our study (0.05 mag). The color term for  $(B - V)$  (Eq. 3) is also small. We thus simplify the above equations to the following, and use them throughout this paper:

$$U - V = 0.087 + 0.8926(u - v) + 0.0274(u - v)^2, \quad (6)$$

$$B - V = b - v, \quad (7)$$

$$U = 0.087 + 0.8926u + 0.1074v + 0.0274(u - v)^2, \quad (8)$$

$$B = b, \text{ and} \quad (9)$$

$$V = v. \quad (10)$$

With this simplification we can compare the instrumental magnitudes  $b$  and  $v$  measured from the UVOT images directly with the Lick calibration, and only need to apply color-term corrections for the  $U$  band. More discussion of the color terms from the observations of SN 2005am can be found in § 5.3.

### 3.2.1. Optimal Aperture Size

What aperture size should one use in the “phot” program, so that the measured instrumental magnitudes are most consistent with the Lick calibration? To answer this question, we performed photometry for the SN 2005am stars using aperture radii of 1 to 25 pixels. As a starting point, we used the zero points for the UVOT filters from Table 1. The measured instrumental  $u$ ,  $b$ , and  $v$  magnitudes are transformed to  $U$ ,  $B$ , and  $V$  according to Eqs. 8–10. Then, for each aperture radius, the difference between the UVOT photometry and the Lick calibration is calculated for each local standard star, the average difference is calculated, and the root-mean-square (RMS) around this average is determined. Since the average difference can be corrected by changing the zero point, the RMS around the average difference measures the degree to which the UVOT photometry is consistent with the Lick calibration.

The DAOPHOT package offers various sky background fitting algorithms; see Stetson (1987) for detailed discussions. In this section, we use a simple “mean” method to determine the sky background in this section. §3.2.4 explores the other algorithms, and concludes that for UVOT observations of SN 2005am, “mean” works best for stars that are not close to other contaminating sources.

Figure 5 shows the RMS versus the aperture size (radius) in pixels. The open circles are for obs1, the solid circles for obs2, the stars for obs3, the solid triangles for obs4, and the solid line for obs5. For obs2 (binned  $2 \times 2$ ), the apertures shown in Figure 5 (APT'; solid circles) are the actual aperture sizes (APT) scaled to match the unbinned data. We found the best match to be  $APT' = APT \times 2 - 1$ , rather than  $APT' = APT \times 2$  as one would expect. The cause of this difference is unclear, but we note that the FWHM of obs2 ( $\sim 2.5$  pixels) is not exactly half of the other unbinned observations (FWHM  $\sim 4.0$  pixels) either.

Figure 5 indicates that for the  $B$  and  $V$  bands, the smallest RMS ( $\sim 0.07$  mag) is achieved with an aperture size of 5 pixels (3 pixels for  $2 \times 2$  binned data). This result is consistent with the trend found in ground-based CCD images, where the best S/N is often achieved when the photometry aperture is slightly bigger than the FWHM. For the  $U$  band, the RMS shows a rather flat distribution for apertures in the range 5–12 pixels.

An aperture size of 12 pixels is used in the *Swift* manual to determine the zero points. As shown in Figure 5, however, the RMS at 12 pixels is 0.04–0.10 mag larger than at 5 pixels (up to 0.15 mag larger in obs3  $V$ ) for the  $B$  and  $V$  bands, and is about the same for both apertures in the  $U$  band.

We thus found that an aperture radius of 5 pixels (3 pixels for  $2 \times 2$  binned data) gives the most consistent results between the UVOT photometry and the Lick calibration of the SN 2005am stars. In sky coordinates, this is  $2''.5$ , and  $3''.0$ , respectively.

### 3.2.2. Zero Points

Ideally, the optimal aperture size also gives the most consistent zero point (a source yielding 1 count per second) for the observations. The average differences as calculated in the previous section, which represent the amount to which the *Swift* zero point in Table 1 needs to be modified when a specific aperture is used, is plotted in Figure 6. The same symbols are used for the different images as in Figure 5.

We note that with the exception of obs3  $V$  (stars in the lower panel) and obs4  $U$

(triangles in the upper panel), the other curves all converge in the aperture size range of 4-8 pixels, then diverge when the aperture is larger or smaller. An aperture size of 5 pixels indeed gives a very consistent zero point for these observations.

Obs4  $U$  is a short exposure (18.02 s), with most of the background having a value of 0; the local standard stars are not well detected. We removed obs4  $U$  from the zero point determination for the  $U$  band, and caution that our preliminary  $U$ -band zero point may not work for short exposures.

We were puzzled by the observation that the well-observed obs3  $V$  gives a different zero point than the other observations. We compared this image to obs1  $V$ . Using a large aperture size of 35 pixels, we measured the total flux for several bright (but without ghost emission) stars, and found that the flux ratios between these stars are inconsistent with the ratio of the exposure times listed in Table 4. From the flux ratios of the stars and the exposure time of obs1  $V$ , the matching exposure time for obs3  $V$  is about 68 s, rather different from 82.77 s as listed in Table 4. It is unlikely that the recorded exposure time is erroneous, and we were unable to find a reasonable explanation to the mysterious deficit of the flux in this image. We thus omit obs3  $V$  from the zero-point determination for the  $V$  band.

With obs3  $V$  and obs4  $U$  excluded from the analysis, we measured the following zero points for the UVOT  $UBV$  filters, when an aperture size of 5 pixels (3 pixels for the  $2 \times 2$  binned data) is used:  $ZP(U) = 18.22 \pm 0.10$  mag,  $ZP(B) = 18.88 \pm 0.09$  mag, and  $ZP(V) = 17.67 \pm 0.07$  mag. These zero points are also listed in Table 5. The uncertainty of the zero point is the quadrature sum of the RMS from the multiple observations and the RMS of the differences between the UVOT photometry and Lick calibration shown in Figure 5.

We also note that when an aperture size of 12 pixels is used, the zero points for the UVOT  $UBV$  filters from our analysis are  $ZP(U) = 18.49 \pm 0.14$  mag,  $ZP(B) = 19.16 \pm 0.20$  mag, and  $ZP(V) = 17.92 \pm 0.18$  mag. These zero points are consistent with those from the *Swift* calibration database as listed in Table 1 to within the quoted errors. Note that the

uncertainties of the zero points with an aperture size of 12 pixels is significantly larger than those with an aperture size of 5 pixels.

### 3.2.3. Zero Points with Correction Factors

In an attempt to further refine the zero points, the residuals of the UVOT photometry when compared to the Lick calibration have been vigorously studied. The UVOT photometry was measured using the optimal aperture size and zero points as discussed above.

In Figure 7, we show the residual of  $B(\textit{Swift}) - B(\text{Lick})$  versus the  $B(\textit{Swift}) - V(\textit{Swift})$  color for the local standard stars in obs1  $B$ . There is no apparent correlation between the residuals and the colors, suggesting that the presence of a large color term is unlikely.

In the upper panel of Figure 8, we show these residuals again, but as a function of  $B(\textit{Swift})$ . A strong correlation can be seen in this plot. To account for this correlation, a correction factor ( $CF$ ) needs to be applied to the magnitudes measured in the “phot” program with zero point of ZP [ $b'(ZP)$ ], i.e.,  $B = b = CF \times b'(ZP)$ . The lower panel of Figure 8 shows that when  $CF = 1.07$  is applied to correct for the measured  $b'$  (with  $ZP = 17.77$  mag), the RMS of the photometry differences is significantly improved, from RMS = 0.082 mag to RMS = 0.035 mag.

We analyzed all the  $B$ -band and  $V$ -band images (except obs3  $V$ ), and a strong dependence of the residuals on the magnitude is apparent for all the images. The correction factors measured from the images are consistent for the same band (to within errors), but are different for the two bands. We thus determine the final correction factors by combining the residuals and magnitudes for all the analyzed images, and measure  $CF(B) = 1.070 \pm 0.009$  and  $CF(V) = 1.046 \pm 0.007$ . The new zero points for the filters (also listed in Table 5) are  $ZP(B, CF) = 17.77 \pm 0.06$  mag, and  $ZP(V, CF) = 16.95 \pm 0.04$  mag. Compared to the ZP without  $CF$  correction, these zero points have smaller uncertainties due to the reduced

RMS between the UVOT photometry and the Lick calibration.

We did not attempt to estimate a correction factor for the  $U$  band because we only have a preliminary  $U$ -band calibration for a limited number of stars. However, since the evaluation of the  $U$  mag involves instrumental magnitude  $v$  (Eq. 8), we calculated the new zero point for the  $U$  band, when the correction factor for  $v$  is used:  $ZP(U, CF) = 18.23 \pm 0.10$  mag.

To investigate the possible causes of the correction factor, and to further understand its properties, we perform the following analyses. First, we check whether the correction factor is related to the magnitude (or count rate for the UVOT detectors) of the stars, or the total counts of the final detection (which is a function of both count rate and exposure time). In the upper panel of Figure 9, we plot the residuals  $B(\text{Swift}) - B(\text{Lick})$  as a function of the  $B(\text{Swift})$  for obs1  $B$  (solid circles) and obs3  $B$  (open circles), whose exposure times differ by a factor of  $\sim 4$  (Table 4). Although the scatter of the points for obs3  $B$  is larger due to its much shorter exposure, the two datasets are consistent with each other. The lower panel of Figure 9 shows these points again, but as a function of the total counts in the photometry apertures. It is clear that the points for obs3  $B$  are systematically offset from these in obs1  $B$ , and we thus conclude that the correction factor is related to the count rate (magnitude) of the stars.

We then check whether the  $CF$  is caused by a systematic effect in evaluating the sky background in our reductions. For example, if our defined sky region is contaminated by the central source, and the contamination is proportional to the brightness of the source, the effect of the contamination on the final photometry may mimic a correction factor. We changed the sky background region to be an annulus with an inner radius of 60 pixels and an outer radius of 80 pixels, and performed photometry for obs1  $B$  again; the results are shown in Figure 10. With such an extensive sky region (the inner radius is  $15 \times \text{FWHM}$ , and is well beyond the rings around the bright stars as seen in Figure 3), we expect the contamination by the central source to be negligible. Figure 10 does not show any significant differences when compared to Figure 8, suggesting that (a) our defined sky region (an annulus from 35 to 45 pixels) is not significantly contaminated by the central source, and (b) the correction

factor is not caused by the sky background determination.

Now we check whether the *CF* is caused by our choice of a relatively small optimal photometry aperture size. In Figure 11, we show the results for photometry performed with larger apertures. With an aperture of 12 pixels (left panel), the correlation between  $B(\textit{Swift}) - B(\textit{Lick})$  and  $B(\textit{Swift})$  is still apparent, and using a *CF* reduces the RMS from 0.116 mag to 0.072 mag. When the aperture is increased to 25 pixels (right panel), there is considerably more scatter in the data points, and using a *CF* does not improve the RMS significantly. However, a weak correlation is still visible. We did not study even larger apertures as the scatter in the data points hides any possible correlations.

One hypothesis is that the *CF* is caused by the fact that the effective PSFs of stars in UVOT images vary as a function of their magnitudes. As a result, when an aperture size is not big enough to sum all the flux for a star, it will collect different fractions of the total flux for stars of different brightness. The measured instrumental magnitudes will then need to be corrected by different amounts for stars of different brightness. To verify this hypothesis, we will need some very deep UVOT images of the SN 2005am field (or other calibrated fields, such as one with many faint Landolt standard stars), so that very big apertures can be used to do photometry without causing the large scatter as seen in the right panel of Figure 11.

We also note that the adoption of the *CF*, which means the correction to the measured instrumental magnitude as a function of the brightness of the source, is similar to the correction caused by dead time or coincidence loss (hereafter CL) for the UVOT detector. Because of the photon-counting nature of the UVOT detector, it can only recognize one photon per detector pixel within each individual frame. For UVOT, this means that sources brighter than  $\sim 20$  counts  $\text{s}^{-1}$  will begin to suffer noticeably from CL, whose correction is directly related to the source brightness. A similar phenomenon for the *XMM-Newton* optical/UV monitor telescope was discussed by Mason et al. (2001). However, CL is only appreciable for bright sources (a count rate of  $> 20$  photons  $\text{s}^{-1}$  corresponds to about  $U < 15$ ,  $V < 15$ , and  $B < 16$  mag), and the majority of the SN 2005am stars have  $B > 16$  mag.

Figure 3 shows that different bright stars show different degrees of “ghost” emission. If the ghost emission exists for all the stars (but is only apparently visible for bright stars), and is proportional to the source brightness, it will introduce a flux loss that is related to brightness. The ghost emission is most likely caused by some internal reflection in the detector, as it is correlated with the bright stars in the field of view. Unfortunately, quantitative information on ghost emissions is not yet available in the *Swift* calibration database.

We emphasize that investigating the cause of the correction factor is beyond the scope of this paper. Since our goal is to empirically find the optimal method to conduct photometry in the UVOT images, and adopting  $CF$  significantly reduces the uncertainties of the results, we consider using  $CF$  an important step in the UVOT photometry.

Table 5 lists the important parameters for doing photometry in the IRAF/DAOPHOT package. A recipe for UVOT photometry can also be found in §3.3.

### 3.2.4. Optimal Sky Fitting Algorithm

At the low background count rates found in the *Swift* UVOT, the distribution of the background in a given aperture is often Poissonian, rather than Gaussian as in ground-based optical images. Because of this, some of the usual sky-fitting routines in IRAF are inappropriate to use. In this section we explore the various sky background fitting algorithms offered by IRAF/DAOPHOT. As discussed in more detail by Stetson (1987), DAOPHOT offers the following sky-fitting methods: constant, file, mean, median, mode, centroid, gauss, ofilter, crosscor, histplot, and radplot. Among these, “constant” and “file” require background values supplied by the user, and are not adopted in our reductions. “Gauss” fits a Gaussian function to the background histograms. As shown in Figure 4 and as discussed in §3.1, most of the histograms do not show a Gaussian distribution, so this method is not used. “Histplot” and “radplot” require the user to mark the background interactively, on the histogram and radial profile plot of the background, respectively. We found it difficult to visually estimate a reasonable background from the plots for many of

the observations, and did not include the results from these two methods in our analysis.

Among the six sky-fitting algorithms we used (mean, median, mode, centroid, ofilter, and crosscor), “mean” often outputs the largest background value, while “centroid” outputs the smallest. The “centroid” method often estimates a background value of 0 (as does the “mode” method), since that is where the histogram peaks for many observations; thus, it produces the brightest star measurements among all the methods.

Using our defined sky background region and the optimal aperture size, we analyze obs1  $V$  using all the six sky-fitting algorithms. We derive the zero points and their uncertainties, and the correction factor for each sky-fitting method, and list the results in Table 6. Without using  $CF$ , all the methods yield consistent zero points and similar uncertainties. The magnitudes measured with the “centroid” method are on average 0.04 mag brighter than with the “mean” method, as indicated by the difference in the zero points. When  $CF$  is used, different methods require slightly different values of  $CF$  (and the associated zero points). The uncertainties of the zero points are very similar, and are also significantly smaller than those without using  $CF$ .

The “mean” method offers a slightly smaller uncertainty than the other methods, and also requires the smallest  $CF$ ; it is thus preferred by us. We note, however, that the results from different sky-fitting methods do not differ significantly in terms of zero-point uncertainties, at least for an uncrowded field such as the SN 2005am stars. In §4, we attempt to derive photometry for SN 2005am in the UVOT images. In this case the different sky-fitting methods yield more significant differences, as SN 2005am is contaminated by a bright nearby star and its host galaxy.

### 3.2.5. *Empirical UVOT Coincidence Loss Correction*

It is important to verify that the photometric parameters we derived from the observations of SN 2005am also work for other UVOT observations. We searched the *Swift* quicklook database, and found a series of  $V$ -band observations for the Landolt standard-star

field “SA104.” A journal of these UVOT observations is presented in Table 7. Quite different exposure times (from 180.04 s to 1146.12 s) were used to make these observations.

We identified all the Landolt standard stars observed in these images, and performed photometry using the parameters discussed in the previous sections, *with CF correction applied*. The residuals of the UVOT photometry and those in the Landolt table (Landolt 1992) are plotted in the upper panel of Figure 12. About 50% of the Landolt stars have magnitudes brighter than 14, and this gives us an opportunity to investigate how to empirically measure photometry for bright stars in the UVOT images. Here we also include reductions for the bright star #6 in the SN 2005am field; these values are shown as stars in the upper panel of Figure 12. To put the data points in context, in the lower panel we show the residuals for all the stars in the SN 2005am field from all the  $V$ -band observations (except obs3  $V$ ).

From the upper panel of Figure 12, it can be seen that our photometric parameters (with *CF* correction) work well for Landolt stars fainter than  $V(Swift) = 14$  mag. The RMS of the residuals for  $V(Swift) > 14$  mag stars is only 0.07 mag, within  $2\sigma$  of the uncertainty of the zero point for the  $V$  band with *CF* correction (0.04 mag). The lower panel also shows that the residuals of the Landolt stars with  $V(Swift) > 14$  mag have a consistent distribution with the stars in the SN 2005am field.

For stars with  $V(Swift) < 14$  mag, however, the measured  $V(Swift)$  shows a dramatically increasing difference from  $V$  as star brightness increases (smaller  $V$ ). This is almost certainly caused by the CL effect for bright stars. We empirically fit a third-order polynomial curve to correct the measured  $V(Swift)$  to  $V$  for stars with  $V(Swift) < 14$  mag, and find the following solution:

$$\Delta V(Swift) = 0.0394 - 0.24644[V(Swift) - 14.0] + 0.320448[V(Swift) - 14.0]^2 - 0.0980155[V(Swift) - 14.0]^3 \quad (11)$$

The RMS for the fit is 0.12 mag for 18 data points. This may be regarded as a first-order correction for the CL effect, before analyses from more bright Landolt stars become

available.

Since there are no UVOT *U*-band or *B*-band images for bright Landolt stars available to us in the archive yet, we attempted to constrain the correction to the CL effect from the only bright star #6 in the SN 2005am field. The upper panel of Figure 13 shows the residuals  $B(\textit{Swift}) - B(\textit{Lick})$  while the lower panel shows  $U(\textit{Swift}) - U(\textit{Lick})$ . Only the datasets with good S/N are included in the *U*-band plot (obs1 *U*, obs2 *U*, and obs5 *U*). Also overplotted are the curves adopted from the fit to the *V* band, but shifted along the magnitude (abscissa) direction by 1.3 mag in *B* and by 0.9 mag in *U*, to visually match the data. Although there are only multiple data points from a single star (#6) at the bright-star end, our limited dataset seems to indicate that our photometric parameters work well for stars with  $B(\textit{Swift}) > 15.3$  mag and  $U(\textit{Swift}) > 14.9$  mag, but stars that are brighter require CL corrections. The very preliminary correction curve from shifting the *V*-band fit has the following solution:

$$\Delta U(\textit{Swift}) = 0.0394 - 0.24644[U(\textit{Swift}) - 14.9] + 0.320448[U(\textit{Swift}) - 14.9]^2 - 0.0980155[U(\textit{Swift}) - 14.9]^3. \quad (12)$$

$$\Delta U(\textit{Swift}) = 0.0394 - 0.24644[U(\textit{Swift}) - 14.9] + 0.320448[U(\textit{Swift}) - 14.9]^2 - 0.0980155[U(\textit{Swift}) - 14.9]^3. \quad (13)$$

Obviously, when more UVOT observations of bright standard stars in the *U* and *B* bands are analyzed, the residual curves at the bright end will be populated by more data points and a better empirical correction formula for the CL effect may be determined.

The long exposure times in im1, im2, and im3 also offer us an opportunity to study the photometry of the Landolt stars using a very large aperture. The results shown in Figure 14 are for photometry performed with an aperture size of 60 pixels, again with *CF* correction applied ( $CF = 1.046$ , and the zero point is changed to 17.43 for such a large aperture). The sky background region is an annulus with an inner radius of 60 pixels and

and outer radius of 80 pixels, and the error bars shown in the figure are the RMS of the photometry using 7 different sky-fitting methods (mean, mode, median, centroid, gauss, ofilter, and crosscor). The “gauss” method is included since the background values in these 3 images are sufficiently high and have a Gaussian-like distribution.

Also overplotted in Figure 14 is the preliminary CL correction curve as derived from Figure 12, but shifted by a small amount (0.15 mag) along the  $V(Swift)$  axis. For the data point marked with a circle, the 60-pixel aperture radius includes another faint source; for the point marked with a square, the edge of the aperture radius is contaminated by another nearby bright source. When these two points are not considered, the other 6 data points for the stars with  $V(Swift) < 14$  mag closely follow our preliminary CL correction curve, and have an RMS of only 0.03 mag. This suggests that for bright and uncrowded sources, it is probably a good idea to use a very big aperture (diameter 60 pixels) and a large sky annulus (60–80 pixels from the source), adopt  $CF = 1.046$  and  $ZP(V) = 17.43$ , and apply the following CL correction:

$$\Delta V(Swift) = 0.0394 - 0.24644[V(Swift) - 14.15] + 0.320448[V(Swift) - 14.15]^2 - 0.0980155[V(Swift) - 14.15]^3 \quad (14)$$

It is possible that the CL effect starts for  $V(Swift) < 15$  mag, as suggested by the pair of data points at  $V(Swift)$  around 14.6 mag. If this is the case, a new curve will need to be fit. Our limited number of data points do not warrant such an exercise, however.

We also note that with a big aperture of 60 pixels, the magnitudes for relatively fainter stars (but still brighter than mag 17) have large error bars, even for images with rather long exposures as we have analyzed here. Thus, photometry with a large aperture is not a viable option for most of the reductions.

### 3.3. Photometry Recipe for the UVOT *UVB* Filters

In this section we summarize the key parameters and steps involved in performing photometry on UVOT *UVB* filters. As using a *CF* improves the uncertainties of the photometric zero points, we only list the procedure when *CF* correction is considered. We list all the important parameters required to do photometry in the IRAF/DAOPHOT package (specifically for the program “phot”), but these should be easily exported to other photometry programs.

1. Input all necessary keywords to the datapars of “phot,” such as “EXPOSURE” as the FITS keyword for the exposure time.
2. The sky region is defined as an annulus with an inner radius of 35 pixels ( $17''.5$ ) and an outer radius of 45 pixels ( $22''.5$ ). That is, in “fitskypars,” annulus = 35, and dannulus = 10. For  $2 \times 2$  binned data, the inner radius becomes 17.5 pixels ( $17''.5$ ) and the outer radius 22.5 pixels ( $22''.5$ ). The preferred sky fitting algorithm is “mean.”
3. The photometry aperture is 5 pixels ( $2''.5$ ) for unbinned data, and 3 pixels ( $3''.0$ ) for  $2 \times 2$  binned data.
4. The photometric zero points are  $ZP(U) = 18.23$ ,  $ZP(B) = 17.77$ , and  $ZP(V) = 16.95$  mag. The uncertainties for these zero points are  $ZPE(U) = 0.10$ ,  $ZPE(B) = 0.06$ , and  $ZPE(V) = 0.04$  mag. When photometry is performed on an object, the final uncertainty should be the zero-point error and the photometry error from “phot” added in quadrature. The photometry measured from this step is denoted as  $u'$ ,  $b'$ , and  $v'$ .
5. The *CF* correction is applied to the photometry from the previous step to derive instrumental magnitudes  $b$  and  $v$ :  $b = CF(b) \times b'$ ,  $v = CF(v) \times v'$ , where  $CF(b) = 1.070 \pm 0.009$ ,  $CF(v) = 1.046 \pm 0.007$ . No *CF* correction is applied to the  $u$  band photometry, so  $u = u'$ .
6. The instrumental magnitudes  $u$ ,  $b$ , and  $v$  are transferred to standard Johnson/Cousins system:

$$U(\textit{Swift}) = 0.087 + 0.8926u + 0.1074v + 0.0274(u - v)^2,$$

$B(\textit{Swift}) = b$ , and

$V(\textit{Swift}) = v$ .

7. If  $U(\textit{Swift}) < 14.9$  mag, the following CL correction should be applied:

$$\Delta U(\textit{Swift}) = 0.0394 - 0.24644[U(\textit{Swift}) - 14.9] + 0.320448[U(\textit{Swift}) - 14.9]^2 - 0.0980155[U(\textit{Swift}) - 14.9]^3.$$

This is a very preliminary correction, and requires refinement with more bright-star observations.

8. If  $B(\textit{Swift}) < 15.3$  mag, the following CL correction should be applied:

$$\Delta B(\textit{Swift}) = 0.0394 - 0.24644[B(\textit{Swift}) - 15.3] + 0.320448[B(\textit{Swift}) - 15.3]^2 - 0.0980155[B(\textit{Swift}) - 15.3]^3.$$

This correction is also very preliminary, and should be used with caution.

9. If  $V(\textit{Swift}) < 14.0$  mag, the following CL correction CL should be applied:

$$\Delta V(\textit{Swift}) = 0.0394 - 0.24644[V(\textit{Swift}) - 14.0] + 0.320448[V(\textit{Swift}) - 14.0]^2 - 0.0980155[V(\textit{Swift}) - 14.0]^3.$$

The RMS of this correction is on the order of 0.12 mag.

#### 4. UVOT Photometry of SN 2005am

In § 3, we used the observations of the SN 2005am stars and some Landolt standard stars, and derived optimal parameters to conduct photometry of UVOT images. In theory, we can simply follow the recipe in § 3.4 and do photometry of SN 2005am in the UVOT images. However, the complex background around the SN (as shown in Figure 1) requires special attention when performing photometry.

As discussed in § 2, in ground-based photometry we used the PSF-fitting technique to fit for the background around the SN and its neighboring bright star, and measured their

fluxes simultaneously. Since the PSF is constant across the image and there are plenty of bright and isolated stars, a robust PSF can be constructed, and the overall photometry shows a high degree of self-consistency; see, for example, the final light curves shown in Figure 2. In UVOT images, however, since the intrinsic PSF is varying, PSF fitting is not possible without a precise description of the intrinsic PSFs. We note that the UVOT observations of the SN 2005am field could be used to study the intrinsic PSFs, but to better constrain the PSF variation dependence on source brightness and position on the chip, many more observations will be needed than those currently available to us. Therefore, we need to resort to aperture photometry to measure the magnitudes of SN 2005am.

Because of the complex background around SN 2005am, it is vital to use a small aperture for photometry, so that the relatively poor sky-background estimate has less impact on the final photometry. Fortunately, our optimal aperture (5 pixels for unbinned data, and 3 pixels for  $2 \times 2$  binned data) is small, and is used to derived photometry for SN 2005am. We also adopt all the other photometric parameters derived from the previous section.

In § 3 we studied several sky-fitting algorithms, and preferred “mean” for uncrowded SN 2005am field stars. However, since our defined sky background region is affected by its host-galaxy emission, “mean” will almost certainly overestimate the background contribution inside the aperture radius. We thus performed photometry on SN 2005am using several sky-fitting algorithms (mean, mode, centroid, median, ofilter, and crosscor), averaging the final results and also calculating their RMS.

The photometry of SN 2005am, as measured both without the  $CF$  correction, and with the  $CF$  correction, is listed in Columns 3 and 4 (respectively) in Table 8. Because we did not include obs4  $U$  (due to its short exposure) and obs3  $V$  (due to its peculiarity as discussed in § 3) in the zero-point determination, we did not perform direct photometry on these images.

Since we have good  $B$  and  $V$ , and preliminary  $U$ , calibrations for part of the SN 2005am UVOT field from the ground, we can also choose to do differential photometry

between the SN and the local standard stars, as shown in Columns 5 and 6 of Table 8. Column 5 is the differential photometry when the star’s instrumental magnitude has not been corrected by  $CF$ , while Column 6 has been corrected by  $CF$ . Depending on the S/N of an individual image, the differential photometry can yield uncertainties bigger or smaller than that from the direct photometry. The uncertainties listed for the direct photometry are the quadrature sums of the following components: the zero-point error, the photometric error from “phot,” and the RMS of different sky-fitting methods. The uncertainties for the differential photometry are the quadrature sums of the “phot” error, the RMS of the different sky-fitting methods, and the RMS of the photometry when compared to all the local standard stars. The zero point and its uncertainty are irrelevant in doing differential photometry. When an image has high S/N, differential photometry offers a smaller uncertainty for the photometry of SN 2005am than direct photometry, as there are many local standard stars in the image which beat down the statistical errors. For obs4  $U$  and obs3  $V$ , differential photometry is the only way to measure the magnitudes for SN 2005am. Comparison of the photometry for SN 2005am from the different methods reveals that there is no significant difference among them, although the differential photometry with  $CF$  correction (Column 6) gives the smallest error bars and is thus preferred by us.

In Column 7 of Table 8, we list the ground-based estimates for the magnitudes of SN 2005am at the time of the UVOT observations by fitting a smooth spline3 (order 2) curve to the the KAIT/Nickel data after JD 2453450, while Column 8 lists the difference between our preferred UVOT photometry of SN 2005am (Column 6) and the ground-based estimate. We also combine the UVOT photometry of SN 2005am with the ground-based Lick light curves in Figure 15, and redo the MLCS2k2 analysis. Overall, the UVOT photometry agrees well with the ground-based estimates, especially for the observations taken in the first 4 sequences. However, the difference in the obs5  $B$  observation,  $-0.44 \pm 0.18$  mag, is quite large. The SN was not well detected in this particular image, and the magnitude may be more seriously affected by the neighboring bright object than in other frames as a result of the short exposure time and poor detection. The parameters in the MLCS2k2 fit for the combined data set do not show any significant changes.

## 5. Discussion

### 5.1. Caveats of Our Photometric Calibrations

Our derived photometric zero points and optimal photometric parameters are entirely empirical. For example, the correction-factor correction and the coincidence-loss correction are derived directly from the data, without considering their exact cause or comparing them to what one would expect from simulations.

The main source of our ground-based photometry comes from the photometric calibration of the SN 2005am stars. Compared to the Landolt (1992) standard-star data that have been obtained by UVOT (the majority of which are not yet available to the general user), the SN 2005am stars have both advantages and disadvantages. The advantages of these stars are as follows:

- (1) They extend the calibration to the fainter end. As can be seen in the lower panel of Figure 12, the Landolt stars are mostly brighter than mag 16, while the SN 2005am stars extend the calibration to mag 18. As the majority of the GRB optical afterglows are expected to be detected much fainter than mag 16, it is critical to study the photometric calibrations at the fainter end.
- (2) There are many local standard stars in each frame. Consequently, the images can be studied one frame at a time, each of which already provides enough information on photometric consistency between the UVOT photometry and the ground-based calibration. The Landolt stars, on the other hand, have a lower density in the UVOT images, especially since many of them are bright and require coincidence-loss correction. It is thus necessary to combine multiple images to get enough statistics, which could introduce unexpected variables that hide the true correlations.

On the other hand, the SN 2005am stars have several disadvantages:

- (1) They do not have the photometric precision of the Landolt stars. The uncertainties of the SN 2005am stars are mostly 0.02-0.03 mag, while those for the Landolt stars are smaller than 0.01 mag.

- (2) They do not cover as wide a color range as the Landolt stars. For example, very blue stars are absent from the SN 2005am stars.
- (3) There are not many calibrated bright stars in the SN 2005am field which could be used to determine the coincidence-loss correction.
- (4) There is only a very preliminary  $U$ -band calibration for a limited number of the SN 2005am stars.

The best-case scenario is to combine the studies of the Landolt star observations with those of the SN 2005am field. This will be possible when more Landolt star observations in the archive become accessible to general users.

Because of the limitations of the SN 2005am stars, and the small number of Landolt star images being tested, it is envisioned that the calibration zero points we derived will be refined in future studies, although we expect the main improvement to be smaller uncertainties for the  $B$  and  $V$  bands and a revised zero point for the  $U$  band. In addition, we used aperture photometry to analyze all the images, and it is conceivable that when software packages have been developed to do intrinsic PSF fitting in the UVOT images, the photometric zero points would change, and better precision could be achieved.

Our study has not explored all of the possible parameters for UVOT observations, such as different binning choices, extremely short and long exposures, etc. We have not correlated the residuals with all possible parameters of *Swift*/UVOT and the detectors either.

Our coincidence-loss corrections should be used with caution, especially for the  $U$  and  $B$  bands where we have only one bright star to provide constraints.

We emphasize that our photometric zero points and optimal photometric parameters may not work well on short ( $< 20$  s) UVOT exposures, as suggested by obs4  $U$ . As it is not always possible to take relatively long exposures with UVOT, it is important to analyze more UVOT images with short exposures to establish their photometric calibrations and optimal photometric parameters. Unfortunately, it is expected that the photometric

calibration for the short exposures suffers from larger uncertainties than those derived in this study, as a shorter exposure time generally means lower S/N. Observing brighter stars in the short exposures to increase the S/N is not an option due to the effect of coincidence loss.

We also note that we did not include obs3  $V$  in our photometric zero-point determinations due to the inconsistency between the flux level and the exposure time in this image. The cause of this inconsistency should be investigated and eliminated, so that future data will not be plagued. The users are urged to seek consistency checks. For example, differential photometry should be performed whenever possible, either instead of the absolute photometry or as a consistency check.

## 5.2. Investigating the Scatter in the UVOT Photometry

It is a bit disappointing that the photometric precision can only be achieved to the 0.05 mag level in our study of *Swift*/UVOT data. Ground-based CCD observations with a moderate-sized telescope can easily reach a precision of 0.02 mag or better for the Landolt standard stars, yet as can be seen in the upper panel of Figure 12, there is a *dispersion* ( $1\sigma$ ) of 0.06–0.07 mag for UVOT observations of Landolt stars with  $V(\textit{Swift}) = 14$  to 16 mag. This scatter is unlikely to be caused by the photometric zero-point errors, as an error in the zero point will cause a constant offset, not scatter. In fact, we believe the reason the zero points still have a relatively large uncertainty (0.04–0.06 mag after the *CF* correction) is because of the scatter in the photometry as demonstrated by these Landolt stars. The lower panel of Figure 12 suggests that the dispersion in the photometry does not change according to the source brightness; thus, the scatter is unlikely to be caused by photon statistics, but rather is intrinsic to the aperture photometry of the UVOT observations.

We note that all raw UVOT images contain systematic modulo-8 fixed-pattern noise (“mod-8 noise” hereafter) as a result of pixel subsampling on the detector. The CCD detector of UVOT has a physical dimension of  $385 \times 288$  pixels, 256  $\times$  256 of which are usable for science observations. The detector attains a large format through a centroiding

algorithm to the incoming photons by subsampling each physical pixel into  $8 \times 8$  virtual pixels, thus providing an image of  $2048 \times 2048$  virtual pixels. This subsampling process introduces faint residuals with a fixed pattern (the mod-8 noise) in the raw UVOT images, which are removed by ground processing (rather than by in-orbit *Swift* processing). The level 2 images we analyzed in our study have been processed by the *Swift* UVOT pipeline, with the mod-8 noise removed. However, as suggested by the *Swift* manual, photometric accuracy is destroyed after removing the fixed-pattern noise, and flux is conserved only within each  $8 \times 8$  pixel block. Moreover, the fixed-pattern noise is modified around bright sources, and cannot be recovered without a well-calibrated Monte Carlo analysis.

It is possible that the dispersion in our aperture photometry is caused by the reduced photometric accuracy after removing the mod-8 noise. Unfortunately, it is impractical to bin the level 2 images by  $8 \times 8$  so that the photometric accuracy can be recovered. The pixel scale would be about  $4''$  after binning, and the photometry would be severely affected by undersampling the PSF of the stars.

To further investigate the effect of the mod-8 noise and its removal in the UVOT photometry, we downloaded the raw images of obs1 *V* and experimented with them using the latest HEAsoft 6.0 software supplied by HEASARC. We kept the images in the detector pixel frame, to avoid possible effects introduced by converting them to the sky coordinate image using “uvotxform.”<sup>3</sup> “Uvotbadpix” was performed to remove bad pixels, “uvotmodmap” was used to remove the mod-8 noises, and “uvotflatfield” was used to remove pixel-to-pixel variation in the image due to detector sensitivity. We also skipped the “uvotmodmap” step and generated an image with the mod-8 noise still included. A difference image was then generated by subtracting the final image with the mod-8 noise removed from the one that skipped “uvotmodmap,” and it represents the total effect on the UVOT images before and after the mod-8 noise is removed by the *Swift* pipeline. In effect, the difference image is the mod-8 noise image normalized by the flat field used in

---

<sup>3</sup>We have performed the same tests on the sky-coordinate images and the results do not change significantly, suggesting that “uvotxform” is not the cause of the photometric scatter.

“uvotflatfield.”

We studied the normalized mod-8 noise image that was applied to obs1  $V$  during our reductions using HEAsoft 6.0. Visual inspection indicates that the image is very flat. When viewed with a large contrast, a faint, large-scale pattern is revealed. When viewed with a small contrast, residuals that correspond to the stars detected in the obs1  $V$  images are apparent. We randomly selected 10,000 position in this image, and summed the flux inside a 5-pixel radius region (the optimal photometric aperture derived from our study) at each location. The histogram of the fluxes from these measurements shows a Gaussian distribution, with a dispersion of only 0.325 counts ( $1\sigma$ ). We also collected the flux inside a 5-pixel radius region centered on each local standard star in the SN 2005am field. The total flux for the SN 2005am stars on the normalized mod-8 noise image has a range from  $-7.74$  to  $+2.67$  counts. Since the total flux for the SN 2005am stars using a 5-pixel photometry aperture has a range of 175–4400 counts, the effect of either the random flux fluctuation ( $\sigma = 0.325$  counts) or the local flux fluctuation ( $-7.74$  to  $+2.67$  counts) on the final photometry is smaller than 0.005 mag, which cannot account for the photometric scatter of 0.04–0.06 mag.

Our analysis also suggests that the mod-8 noise removal procedure as implemented in HEAsoft 6.0 has negligible effect on the final photometry of most stars. Only the faintest stars that are close to the detection limit will suffer from the flux fluctuation of  $\sigma = 0.325$  counts (the flux fluctuations for the SN 2005am stars are larger, but they are rather bright stars). In fact, when the raw image of obs1  $V$  is studied, it yields nearly the same RMS as the processed image with mod-8 noise removed. The reasons for this are that (1) there are not many bad pixels in the UVOT detector, (2) the flat field is nearly a constant 1, and (3) the mod-8 noise removal does not change the photometry significantly.

We experimented with artificially smoothing the images by a small amount. When obs1  $V$  is convolved with an elliptical Gaussian function with  $\sigma = 1.0$  and 1.5 pixels, the photometric RMS can be slightly improved by about 0.005 mag. As this is not a dramatic improvement, and smoothing (especially with a high  $\sigma$ ) will change the zero points at specific photometric aperture radius, we did not re-analyze all the data after some artificial

smoothing.

We tried to correlate the scatter in the photometry with the coordinates of the stars on the images, but found no apparent trend.

It is important to remove the photometric scatter to improve the photometric accuracy of UVOT images, either through finding the cause of the scatter from observations and subsequent pipeline reductions, or by searching for more sophisticated photometric methods than the aperture photometry method we have employed in our study. When the intrinsic PSF variation has been established from more on-flight observations, for example, the PSF-fitting technique may be applied and may yield better photometric precision.

### 5.3. $B - V$ Color Term from the SN 2005am Observations

To simplify the analysis in our study, we did not consider color-term corrections for the UVOT  $B$  or  $V$  filters. Here we verify that this simplification is valid, at least for the current photometric accuracy we can achieve with the UVOT observations. In Figure 16 we show the residuals of  $(B - V) - (b - v)$  versus  $(b - v)$ , where  $(B - V)$  are the colors from the Lick calibration, and  $(b - v)$  are the instrumental colors (after the  $CF$  correction) from the UVOT photometry. We only studied the sequences that have excellent images in both  $B$  and  $V$  bands: obs1 (solid circles) and obs2 (open circles). We also overplotted three fitting functions in Figure 16. The solid line is  $(B - V) = (b - v)$ , which is used in this paper. The dashed line is  $(B - V) = 1.0148(b - v) - 0.032$ , which is adopted from the *Swift* manual, but with the curve shifted to match our reductions. The dot-dashed line is our best fit to the data points:  $(B - V) = 0.919(b - v) + 0.076$ . The RMS for the three fits are 0.096 mag, 0.101 mag, and 0.067 mag, respectively.

We note that although our best fit (dot-dashed curve) achieved the smallest RMS, the fit is dominated by just one star (two points) at the red color end, and by the larger scatter in the  $2 \times 2$  binned obs2 (open circles) at the blue color end. The data points in obs1 agree well with the simple  $(B - V) = (b - v)$ , with an RMS of 0.058 mag. The RMS from

adopting the color term from the *Swift* manual is slightly worse than the other two fits. We emphasize, however, that the three fits do not differ significantly from one another within the limited color range of our reductions.

To summarize, unless the UVOT photometric precision can be significantly improved, our data suggest that no color-term corrections for the UVOT *B* and *V* bands are necessary.

## 6. Conclusions

In this paper we present an empirical determination of the optimal photometric parameters to analyze UVOT images using software tools that are familiar to ground-based optical astronomers, and the zero points and their uncertainties in the UVOT *U*, *B*, and *V* filters. We focused our analysis on the calibrated local standard stars in the SN 2005am field, but verified the parameters on a limited number of Landolt standard-star observations. Within the limitations as detailed in § 5.1, the main conclusions from our analysis are as follows:

1. The optimal aperture radius to do UVOT photometry, such that the results are most consistent with the ground-based calibration, is small. A radius of 5 UVOT pixels should be used for unbinned data, and 3 pixels for the  $2 \times 2$  binned data. This is  $2''.5$  and  $3''.0$  in sky coordinates, respectively.
2. The uncertainty of the photometric zero points can be significantly improved when a correction factor is applied to the instrumental magnitudes measured from UVOT images. The final zero point uncertainties are 0.10 mag for *U*, 0.06 mag for *B*, and 0.04 mag for *V*.
3. For very bright stars, the effect of the coincidence loss is apparent in our reductions, and we derived an empirical correction to the *V* band. Corrections to the *U* and *B* bands are presented as well, but they are very preliminary.

4. There is an intrinsic scatter on the order of 0.04–0.06 mag in the aperture UVOT photometry that cannot be easily explained or removed. To further improve the UVOT photometric precision, either the cause of the scatter must be found and fixed, or more sophisticated photometric procedures than simple aperture photometry need to be developed.
5. The color terms of the UVOT  $B$  and  $V$  are small, and need not to be considered unless the UVOT photometric precision is significantly improved.
6. It is important to analyze more UVOT images with short exposures to verify that they can be processed using the derived photometric calibrations and optimal photometric parameters.
7. In § 3.4 of the paper, we offer a step-by-step photometry procedure for UVOT images, including all the optimal photometric parameters and their associated errors.
8. We performed photometry of SN 2005am in the UVOT images, and compared the results with those from ground-based observations. The UVOT photometry is generally consistent with the ground-based observations, but the difference can be up to 0.4–0.5 mag when the SN is faint.

Based on our study of the photometry of UVOT images, we offer the following suggestions for future *Swift*/UVOT observations and calibrations. We advise that on-board binning be avoided for the UVOT observations. Though we were able to analyze the  $2 \times 2$  binned data, the binning introduces yet another variable in the uncertainties of the photometric zero points. Many photometric calibration observations should be performed not only of bright Landolt stars, but also of stars at the fainter end, perhaps to an even fainter level than we have studied in this paper ( $V \approx 18$  mag). These calibrations should also be done with exposure times that span a large range, including very short durations ( $< 20$  s). Series of observations of the same object should be obtained by varying the pointing so the object is detected at different positions on the chip, to better constrain the uncertainty caused by the PSF variation across the chip.

The work of A.V.F is supported by National Science Foundation grant AST-0307894 and NASA/*Swift* grant NNG05GF35G; he is also grateful for a Miller Research Professorship at U.C. Berkeley, during which part of this work was completed. KAIT was made possible by generous donations from Sun Microsystems, Inc., the Hewlett-Packard Company, AutoScope Corporation, Lick Observatory, the National Science Foundation, the University of California, and the Sylvia & Jim Katzman Foundation.

## REFERENCES

Bertin, E., & Arnouts, S 1996, A&A, 117, 393

Filippenko, A. V. 2003, in *From Twilight to Highlight: The Physics of Supernovae*, ed. W. Hillebrandt and B. Leibundgut (Berlin: Springer-Verlag), 171

Filippenko, A. V., et al. 1992, AJ, 104, 1543

Filippenko, A. V., Li, W., Treffers, R. R., & Modjaz, M. 2001, in Small-Telescope Astronomy on Global Scales, ed. W.-P. Chen, C. Lemme, & B. Paczyński (ASP Conf. Ser. 246; San Francisco: ASP), 121

Jha, S. 2002, PhD thesis, Harvard University

Jha, S., Riess, A. G., & Kirshner, R. P. 2005b in prep

Jha, S., et al., 2005a, AJ, in press

Landolt, A. U. 1992, AJ, 104, 340

Li, W., et al. 2000, in *Cosmic Explosions*, ed. S. S. Holt & W. W. Zhang (New York: American Institute of Physics), 103

Li, W., et al., 2003, PASP, 115, 453

Modjaz, M., Kirshner, R., & Challis, P., 2005, IAU Circ. 8491

Martin, R., Yamaoka, H., & Itagaki, K. 2005, IAU Circ. 8490

Mason, K. O., et al., 2001, A&A, 365, L36

Stetson, P. B. 1987, PASP, 99, 191

Table 1. Zero points (ZP; mag) for various *Swift*/UVOT filters from the *Swift* CALDB

Filter	<i>U</i>	<i>B</i>	<i>V</i>	<i>UVW1</i>	<i>UVW2</i>	<i>UVM2</i>
ZP	18.34	19.12	17.83	17.82	17.82	17.19
Error	0.16	0.08	0.09	0.23	0.27	0.26
Aperture (pixels)	12	12	12	35	35	35

Table 2. Photometry of local standard stars in the field of SN 2005am

ID	<i>U</i>	<i>N<sub>U</sub></i>	<i>B</i>	<i>N<sub>B</sub></i>	<i>V</i>	<i>N<sub>V</sub></i>	<i>R</i>	<i>N<sub>R</sub></i>	<i>I</i>	<i>N<sub>I</sub></i>
1	–	–	17.62(01)	2	16.71(03)	3	16.15(01)	2	15.82(02)	2
2	16.80(05)	1	16.90(01)	2	16.39(02)	3	16.08(02)	2	15.75(02)	2
3	–	–	18.12(02)	3	17.37(02)	3	16.84(01)	2	16.49(03)	4
4	16.78(05)	1	15.59(01)	2	14.55(02)	2	13.73(01)	2	13.24(01)	2
5	17.16(05)	1	17.14(01)	2	16.56(02)	3	16.13(02)	2	15.79(02)	3
6	12.39(05)	1	12.30(02)	4	11.99(01)	3	11.78(03)	3	11.58(02)	2
7	–	–	18.20(01)	2	17.22(03)	4	16.55(03)	3	16.07(03)	2
8	–	–	18.75(01)	2	17.81(03)	1	17.22(03)	2	16.66(03)	1
9	–	–	17.79(02)	3	17.23(03)	2	16.96(03)	3	16.63(01)	3
10	–	–	17.94(01)	4	17.09(02)	2	16.51(01)	2	15.93(01)	2
11	–	–	18.16(01)	2	17.29(01)	2	16.70(03)	2	16.46(03)	2
12	16.15(05)	1	15.57(03)	4	14.76(01)	3	14.30(02)	2	13.88(01)	2
13	–	–	19.03(03)	1	17.63(03)	1	16.67(02)	2	15.79(02)	2
14	–	–	17.38(03)	3	16.53(01)	2	16.12(01)	3	15.75(02)	4
15	–	–	16.73(01)	2	15.95(03)	1	15.56(03)	2	15.13(03)	1
16	–	–	17.73(01)	3	17.13(02)	3	16.71(03)	3	16.40(02)	4
17	–	–	17.43(01)	2	16.77(03)	1	16.39(01)	2	16.03(03)	2
18	–	–	17.62(01)	4	16.91(02)	4	16.50(03)	4	16.16(02)	4
19	–	–	18.35(02)	2	17.40(02)	4	16.83(02)	4	16.37(03)	4
20	–	–	17.31(01)	4	16.55(03)	3	16.12(03)	3	15.71(02)	4
21	16.22(05)	1	15.55(01)	4	14.70(02)	4	14.22(02)	3	13.76(02)	4
22	15.02(05)	1	14.98(01)	4	14.47(03)	3	14.18(03)	4	13.90(02)	4
23	–	–	18.02(01)	2	17.35(02)	4	16.97(02)	4	16.59(01)	4
24	–	–	17.48(01)	2	16.54(02)	4	15.93(01)	4	15.45(02)	4
25	16.05(05)	1	15.73(01)	4	15.00(02)	4	14.59(01)	4	14.23(02)	4
26	–	–	16.49(02)	4	15.38(02)	4	14.68(01)	4	14.12(01)	4
27	–	–	17.20(03)	1	16.30(02)	2	15.83(01)	2	15.37(01)	2
28	–	–	17.60(02)	2	16.98(01)	2	16.60(04)	2	16.23(04)	2

Note: uncertainties are indicated in parentheses.

Table 3. Lick Observatory photometry of SN 2005am

JD – 2450000	<i>U</i> (mag)	<i>B</i> (mag)	<i>V</i> (mag)	<i>R</i> (mag)	<i>I</i> (mag)	Tel.
3435.83	—	—	—	13.73(03)	13.90(03)	KAIT
3436.76	—	13.90(04)	13.80(04)	13.70(04)	13.93(05)	KAIT
3438.74	—	13.92(02)	13.75(03)	13.65(03)	13.96(04)	KAIT
3439.77	—	13.98(02)	13.78(02)	13.66(03)	13.97(03)	KAIT
3440.74	—	14.04(03)	13.79(03)	13.69(03)	14.01(04)	KAIT
3441.75	—	14.10(02)	13.81(03)	13.73(02)	14.03(02)	Nickel
3442.69	—	14.18(03)	13.84(03)	13.82(04)	14.15(05)	KAIT
3443.76	—	14.27(02)	13.89(03)	13.90(02)	14.18(02)	Nickel
3444.73	—	14.37(03)	13.95(03)	13.99(02)	14.26(03)	Nickel
3444.76	—	14.43(03)	13.98(04)	14.03(03)	14.32(05)	KAIT
3445.77	—	14.53(02)	14.05(02)	14.10(05)	14.39(03)	KAIT
3446.75	—	—	14.12(04)	—	—	KAIT
3455.75	—	15.90(04)	14.72(03)	14.39(04)	14.21(03)	KAIT
3460.73	—	16.46(02)	15.17(02)	14.76(03)	14.42(04)	KAIT
3462.73	—	16.59(02)	15.35(02)	14.97(03)	14.61(03)	KAIT
3465.70	—	16.78(02)	15.55(04)	15.21(03)	14.88(05)	KAIT
3466.69	17.02(0.08)	16.86(05)	15.62(04)	15.21(04)	14.96(06)	KAIT
3467.73	—	16.87(03)	15.65(03)	15.30(03)	15.05(04)	KAIT
3470.77	—	16.99(02)	15.77(03)	15.38(05)	15.09(04)	Nickel
3471.68	—	17.01(03)	15.79(04)	15.47(02)	15.15(03)	Nickel
3471.68	—	17.02(03)	15.81(05)	15.49(04)	15.25(05)	KAIT
3472.73	—	17.01(03)	15.91(03)	15.57(04)	15.39(04)	KAIT
3474.71	—	17.10(03)	15.92(04)	15.64(03)	15.44(04)	KAIT
3477.67	—	17.15(05)	16.03(06)	15.75(04)	15.58(06)	KAIT
3486.66	—	17.40(04)	16.31(03)	16.06(03)	16.02(03)	KAIT
3492.67	—	—	—	16.30(03)	—	KAIT

Note: uncertainties are indicated in parentheses.

Table 4. Journal of *Swift*/UVOT observations of SN 2005am in *UBV*

Data ID	Obs ID	Date	Filter	UT Start	Exp. time(s)
obs1	sw00030010070	2005-04-04	<i>U</i>	11:38:44	201.76
			<i>B</i>	11:42:14	169.41
			<i>V</i>	11:18:09	201.77
obs2 <sup>a</sup>	sw00030010071	2005-04-06	<i>U</i>	08:39:02	209.77
			<i>B</i>	08:42:39	144.23
			<i>V</i>	08:28:12	209.77
obs3	sw00030010072	2005-04-10	<i>U</i>	02:23:41	82.78
			<i>B</i>	02:25:10	40.61
			<i>V</i>	02:15:04	82.77
obs4	sw00030010073	2005-04-22	<i>U</i>	02:24:07	18.02
			<i>V</i>	02:08:03	157.78
obs5	sw00030010076	2005-05-17	<i>U</i>	03:22:59	72.78
			<i>B</i>	03:25:04	46.68
			<i>V</i>	03:15:29	72.77

<sup>a</sup>These data are binned 2×2.

Table 5. Aperture photometry parameters for *Swift*/UVOT<sup>a</sup>

Parameter	Value
Sky region	35–45 pixels (17.5–22.5 for $2\times 2$ binned data)
Sky fitting algorithm	mean (but see text for crowded regions)
Aperture size	5 pixels (3 pixels for $2\times 2$ binned data)
$ZP(U)$	$18.26 \pm 0.10$
$ZP(B)$	$18.88 \pm 0.09$
$ZP(V)$	$17.67 \pm 0.07$
$ZP(U, CF)$	$18.27 \pm 0.10$ ; $CF = 1.046$ for $V$
$ZP(B, CF)$	$17.77 \pm 0.06$ ; $CF = 1.070$
$ZP(V, CF)$	$16.95 \pm 0.04$ ; $CF = 1.046$

<sup>a</sup>See § 3.4 for a complete recipe on how to use these parameters to do photometry on UVOT images.

Table 6. Comparison of different sky background fitting algorithm for obs1  $V$ 

Algorithm	Without $CF$		With $CF$		
	ZP	$\sigma(ZP)$	$CF$	ZP	$\sigma(ZP)$
mean	17.68	0.067	1.046	16.95	0.043
mode	17.69	0.074	1.060	16.77	0.044
median	17.69	0.072	1.060	16.76	0.043
centroid	17.73	0.094	1.090	16.38	0.049
ofilter	17.69	0.073	1.060	16.76	0.043
crosscor	17.70	0.078	1.070	16.63	0.044

Table 7. Journal of *Swift*/UVOT observations of the Landolt standard star field “SA104”

Data ID	Obs ID	Date	Filter	UT Start	Exp. time(s)
im1	sw00055400016	2005-04-19	<i>V</i>	17:53:57	1146.12
im2	sw00055450010	2005-04-19	<i>V</i>	18:13:26	697.78
im3	sw00055450008	2005-04-05	<i>V</i>	08:11:46	737.52
im4	sw00055350013	2005-05-10	<i>V</i>	01:20:03	180.04

Table 8. *Swift*/UVOT photometry of SN 2005am

JD – 2450000	Filter	Mag1 <sup>a</sup> (mag)	Mag2 <sup>b</sup> (mag)	Mag3 <sup>c</sup> (mag)	Mag4 <sup>d</sup> (mag)	Mag(Lick) <sup>e</sup> (mag)	Diff. <sup>f</sup> (mag)
3464.986	<i>U</i>	17.02(11)	17.02(11)	17.04(08)	17.03(07)		
3464.989	<i>B</i>	16.86(10)	16.85(07)	16.85(09)	16.83(05)	16.73(03)	0.10(06)
3464.973	<i>V</i>	15.53(08)	15.49(05)	15.54(07)	15.49(05)	15.50(02)	-0.01(05)
3466.862	<i>U</i>	17.03(11)	17.03(11)	17.07(11)	17.06(10)	17.02(08)	0.04(13)
3466.864	<i>B</i>	16.86(10)	16.86(08)	16.88(09)	16.87(07)	16.86(05)	0.01(09)
3466.855	<i>V</i>	15.55(08)	15.51(05)	15.54(06)	15.51(05)	15.62(04)	-0.11(06)
3470.600	<i>U</i>	17.16(13)	17.16(13)	17.20(10)	17.20(09)		
3470.601	<i>B</i>	16.97(12)	16.97(10)	16.97(11)	16.97(10)	16.99(02)	-0.02(10)
3470.594	<i>V</i>			15.80(12)	15.78(10)	15.77(03)	0.01(10)
3482.600	<i>U</i>			17.48(17)	17.48(16)		
3482.590	<i>V</i>	16.20(09)	16.20(07)	16.20(07)	16.20(05)	16.18(04)	0.02(06)
3507.641	<i>U</i>	18.16(19)	18.16(19)	18.16(19)	18.17(19)		
3507.642	<i>B</i>	17.48(16)	17.52(14)	17.47(18)	17.50(16)	17.94(08)	-0.44(18)
3507.636	<i>V</i>	16.84(16)	16.86(13)	16.83(17)	16.85(17)	17.02(06)	-0.17(18)

<sup>a</sup>Magnitude measured with the ZP in Table 6, without using *CF*.

<sup>b</sup>Magnitude measured with the ZP in Table 6, with *CF* applied.

<sup>c</sup>Magnitude measured from differential photometry, without using *CF*.

<sup>d</sup>Magnitude measured from differential photometry, with *CF* applied.

<sup>e</sup>Magnitude measured (or extrapolated) from Lick Observatory observations.

<sup>f</sup>The difference between Column 6 and Column 7.

Fig. 1.— A KAIT *R*-band image taken on 2005 Mar. 13 (left) and a Nickel *R*-band image taken on 2005 Mar. 12 (right). The field of view of KAIT is  $6'.6 \times 6'.6$ , and it is  $6'.3 \times 6'.3$  for Nickel. North is up and east is to the left. The local standard stars listed in Table 2 are labeled.

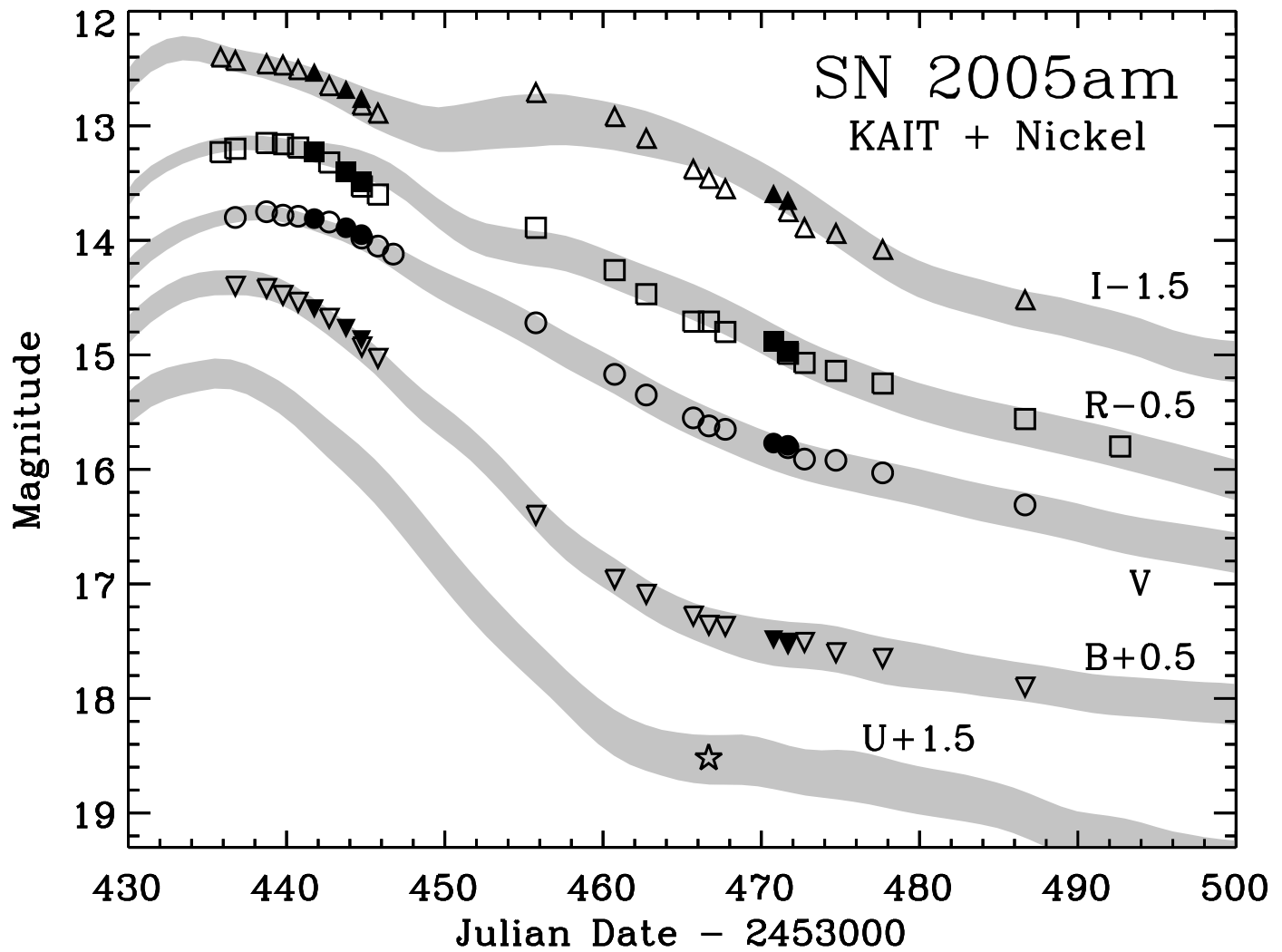


Fig. 2.— The ground-based photometry of SN 2005am. The solid symbols are from Nickel, and the open symbols are from KAIT. Also overplotted are the MLCS fits.

Fig. 3.— Sample PSFs of stars on the UVOT obs1 *V* image. (1) A very bright star with ghost wings (a), ghost ring (b), and ring (c); (2) a pair of bright stars with ghost rings (b) and rings (c); (3) a bright star with ring (c); and (4) stars with no ghost emission, but with varying profiles.

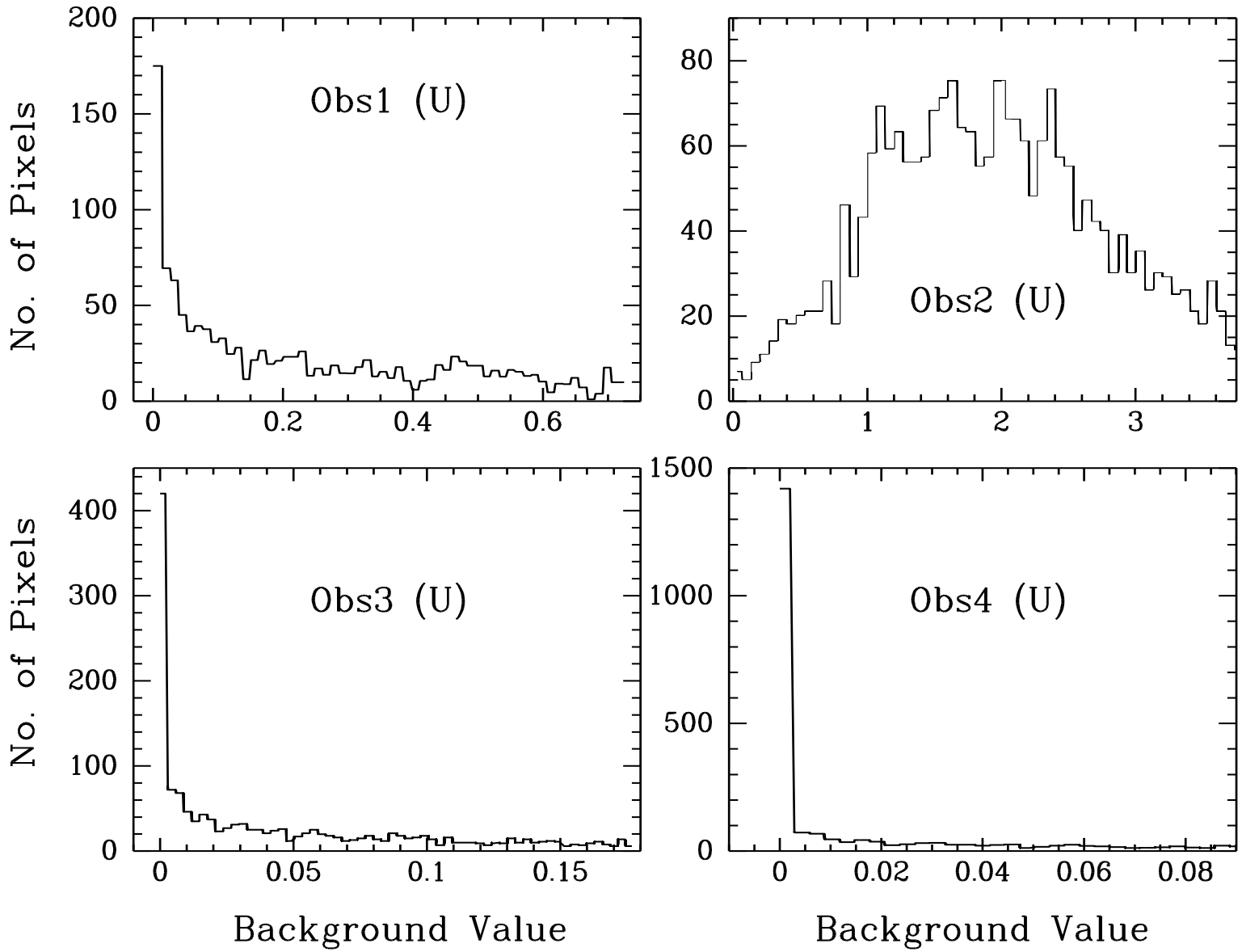


Fig. 4.— The histogram of sky background around Star #5 in the four  $U$ -band observations. Only obs2 has a Gaussian-like distribution. The other distributions peak and truncate at a zero sky value.

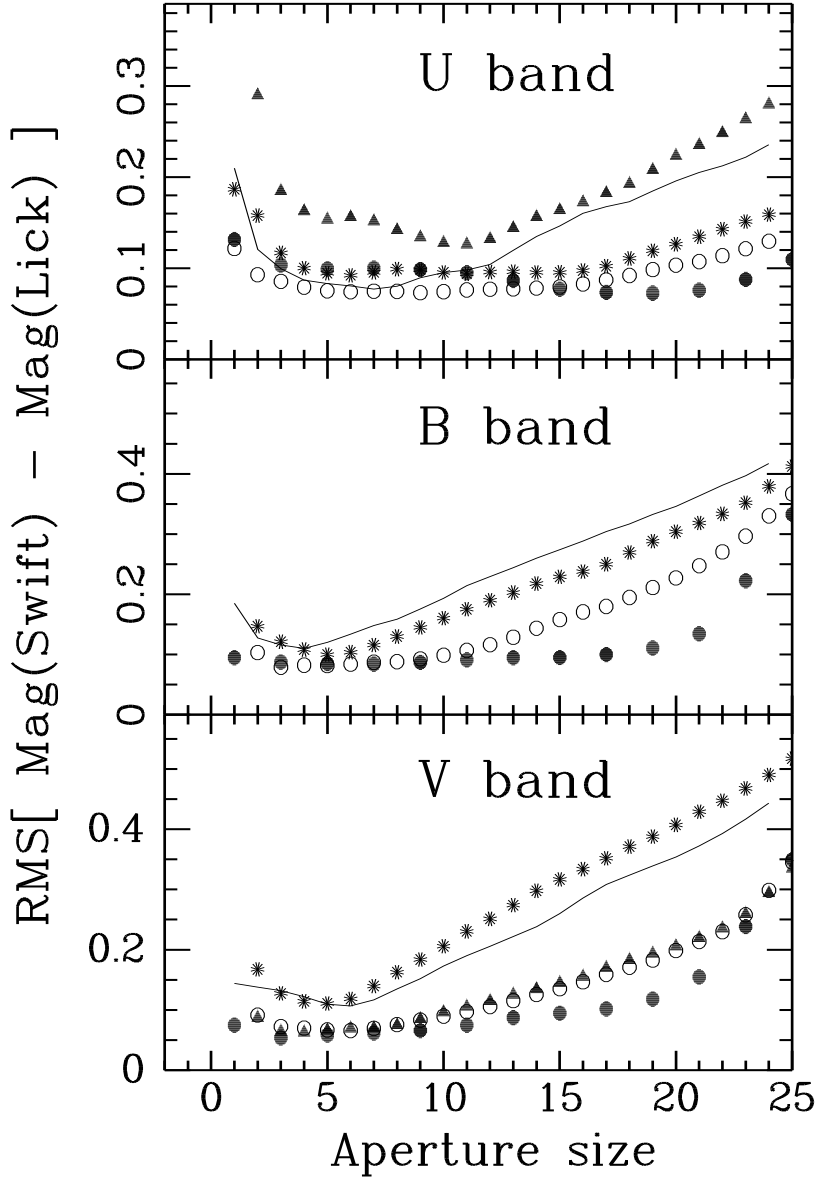


Fig. 5.— The RMS of the differences between the UVOT photometry and the Lick calibrations, as a function of aperture size. Obs1 is shown as open circles, obs2 as solid circles, obs3 as stars, obs4 as solid triangles, and obs5 as solid lines. For obs2, the apertures are displayed as  $APT(\text{used}) \times 2 - 1$ . The smallest RMS is achieved when an aperture radius of 5 pixels (3 pixels for  $2 \times 2$  binned data) is used to do photometry for the  $B$  and  $V$  bands. The  $U$ -band RMS has a flat distribution for aperture sizes in the 5–11 pixel range.

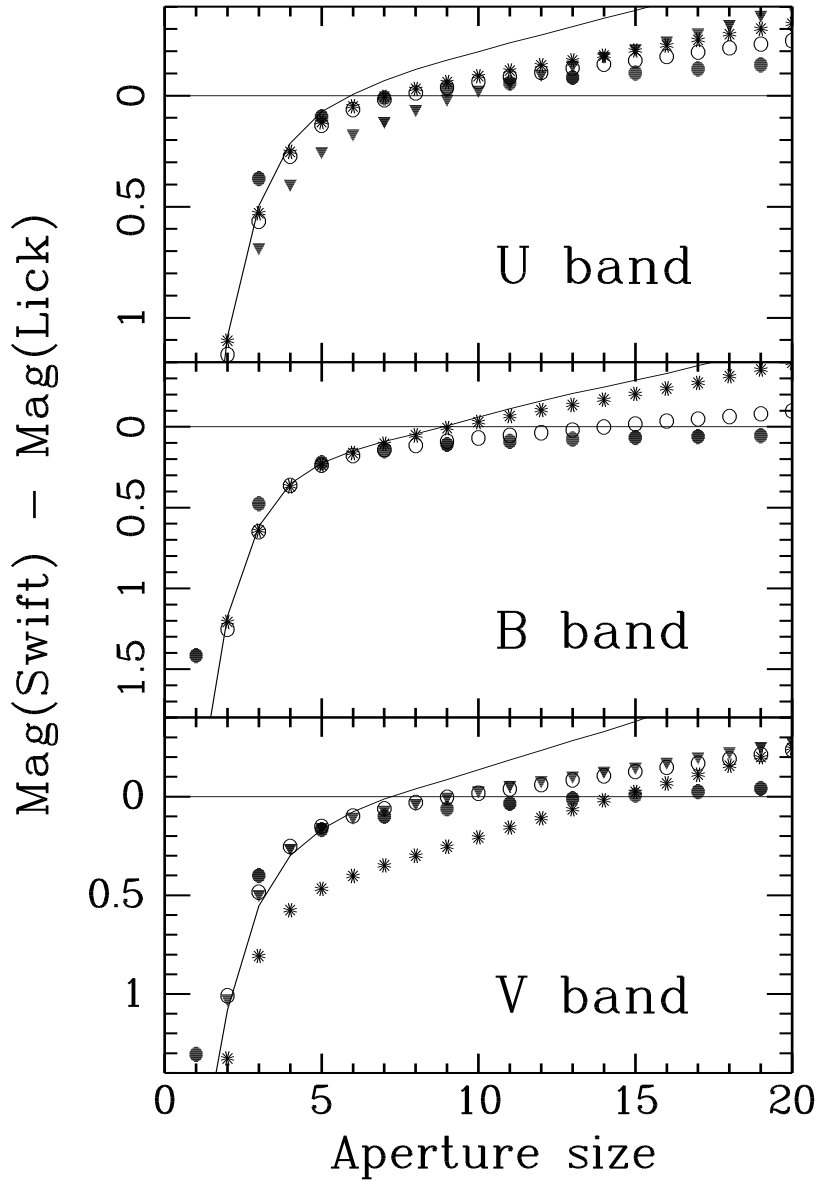


Fig. 6.— The difference between the UVOT photometry and the Lick calibrations, as a function of aperture size. The same symbols have been used as in Figure 5.

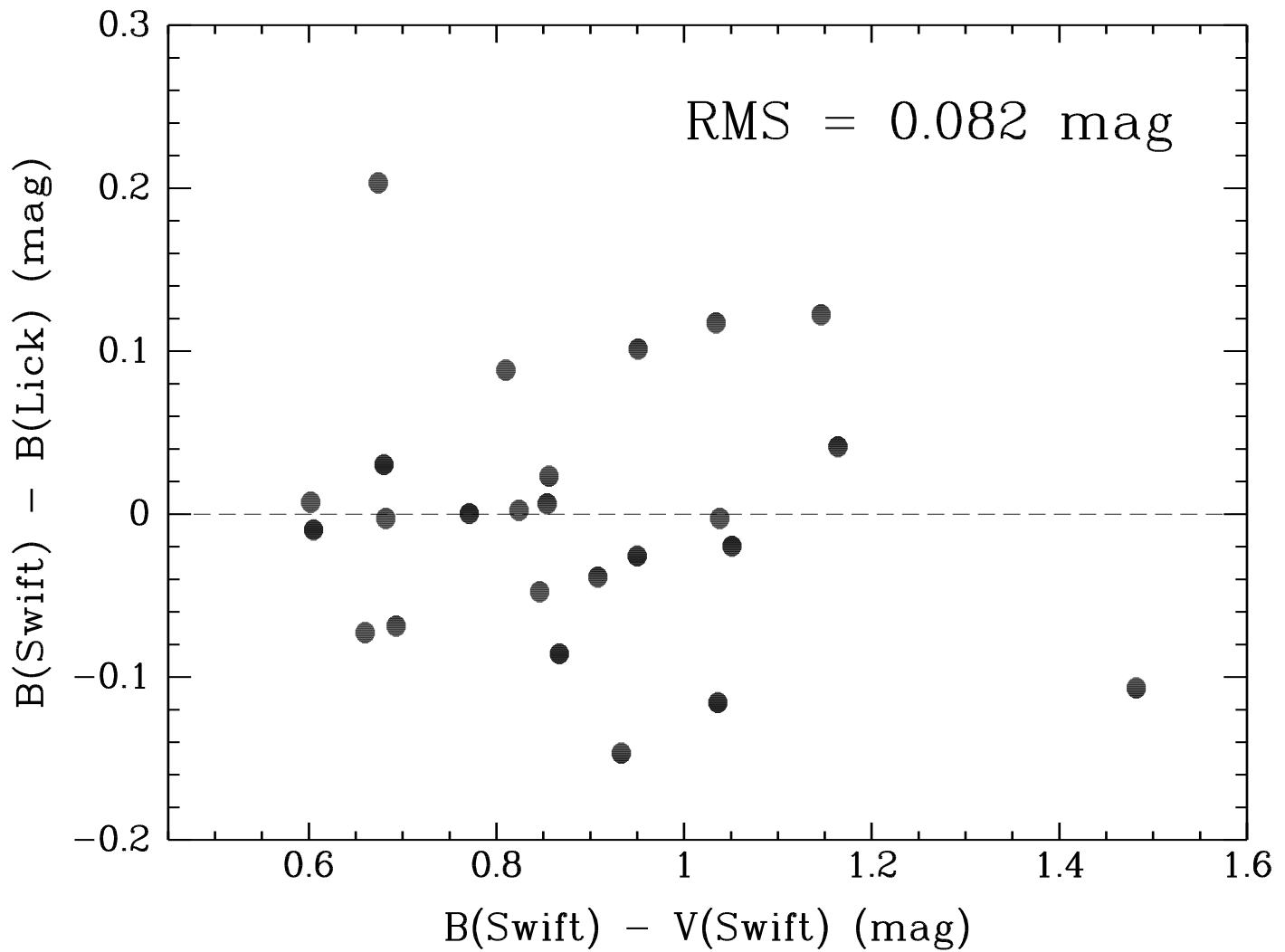


Fig. 7.— The residual  $B(\text{Swift}) - B(\text{Lick})$  versus the  $B(\text{Swift}) - V(\text{Swift})$  color in obs1  $B$ . The RMS is 0.082 mag, and there is no apparent correlation between the residuals and the colors.

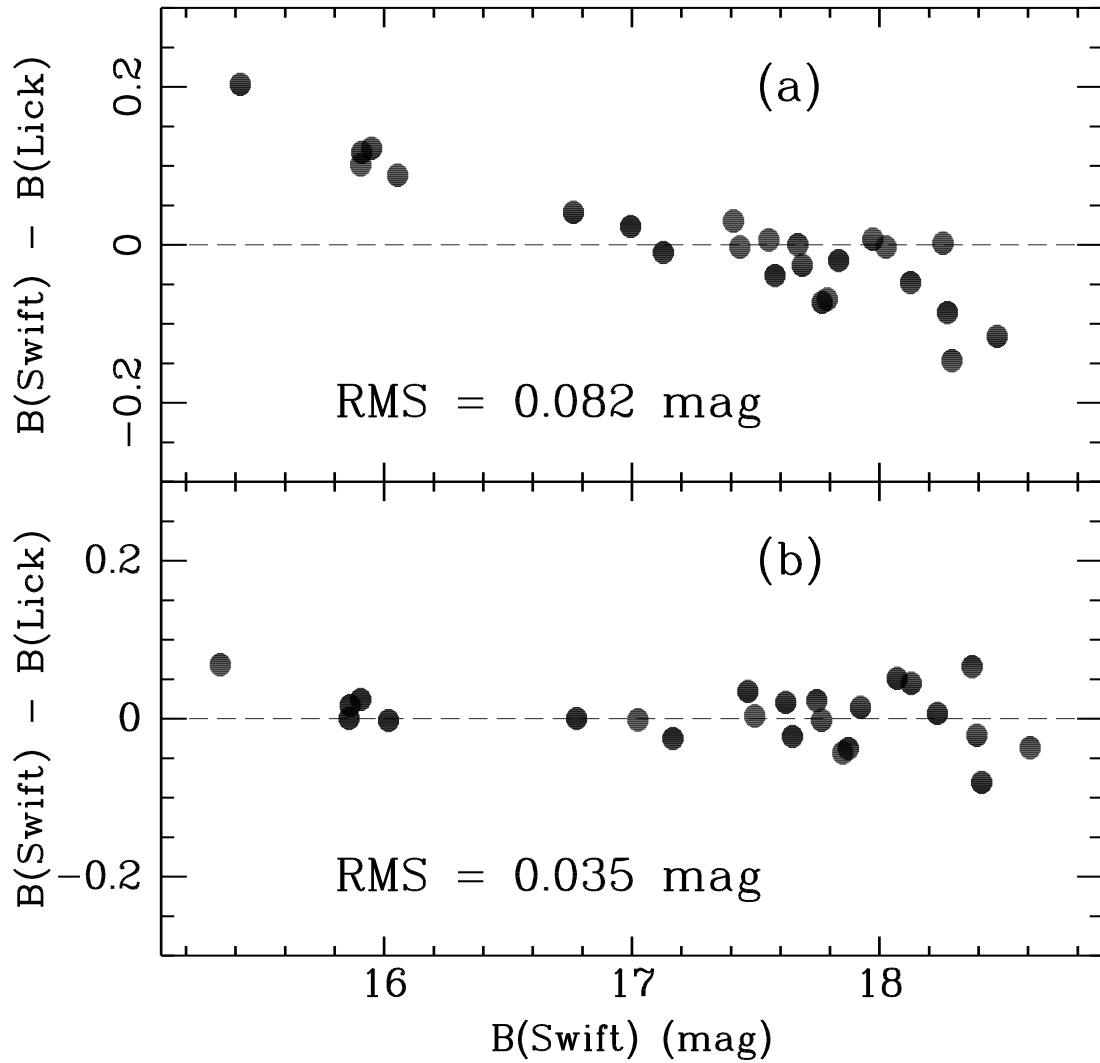


Fig. 8.— Upper panel: the residual  $B(\text{Swift}) - B(\text{Lick})$  versus the magnitude  $B(\text{Swift})$  in obs1  $B$ , which shows a strong correlation. Lower panel: After the correlation is removed, the RMS is significantly improved.

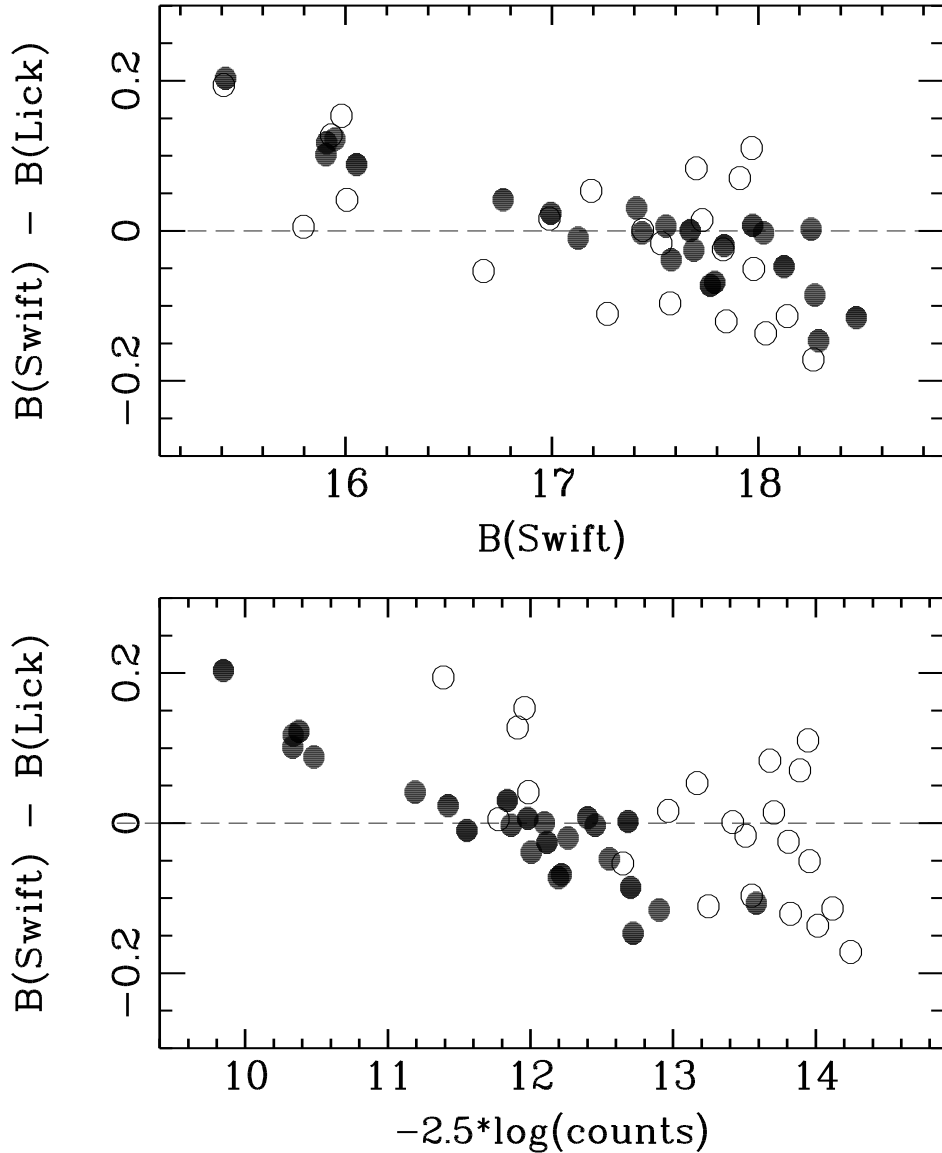


Fig. 9.— Upper panel: the residual  $B(\text{Swift}) - B(\text{Lick})$  versus the magnitude  $B(\text{Swift})$  in obs1  $B$  (solid circles) and obs3  $B$  (open circles). Obs3  $B$  shows a larger scatter due to its short exposure time. Lower panel: the residual  $B(\text{Swift}) - B(\text{Lick})$  versus the number of counts in the photometric aperture. The offset between the open and filled symbols (with differing exposure times) shows that the residual is correlated with the stellar magnitudes, not the total number of counts.

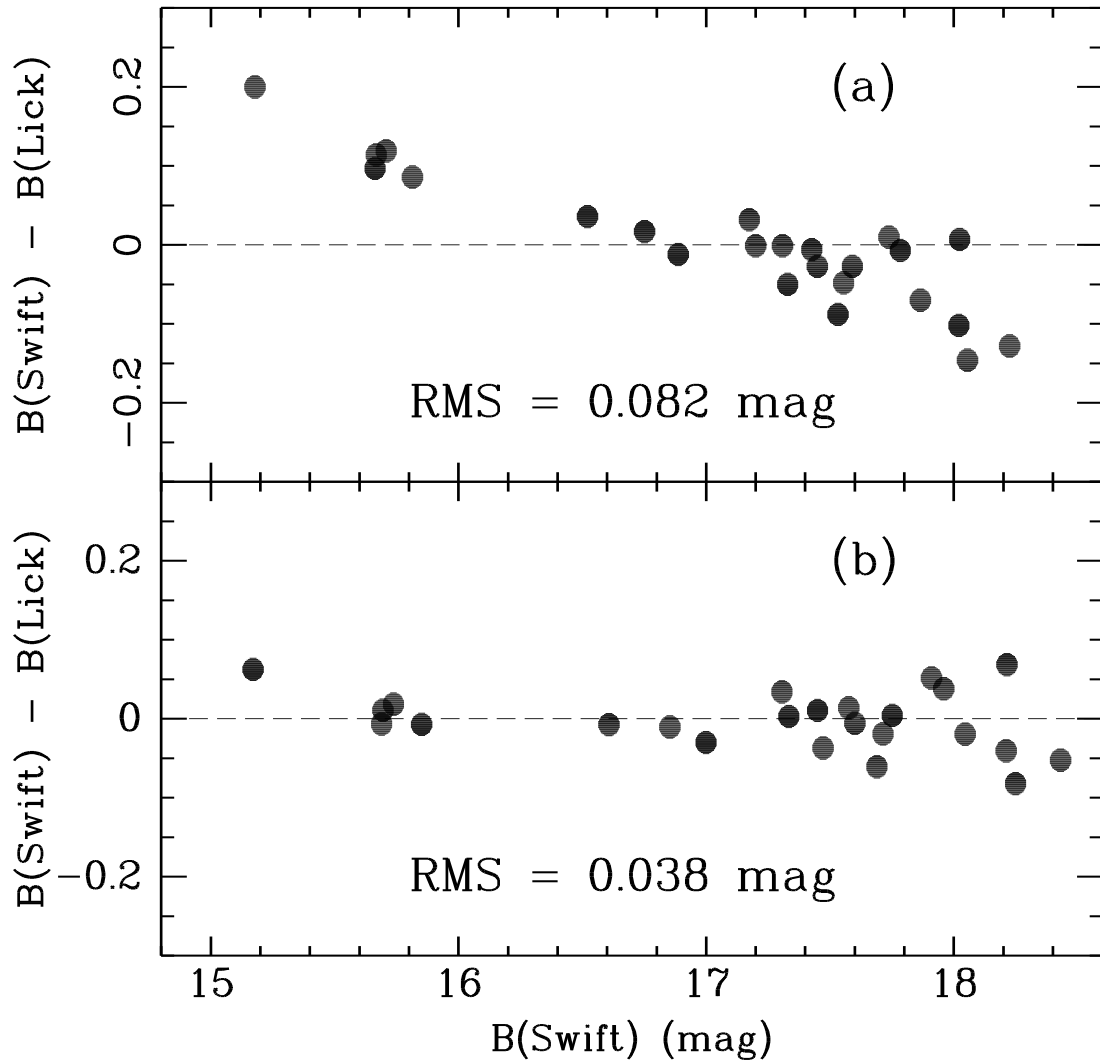


Fig. 10.— Same as Figure 8, but with the sky region now defined as an annulus with an inner radius of 60 pixels and an outer radius of 80 pixels. A bigger sky region does not change the results significantly.

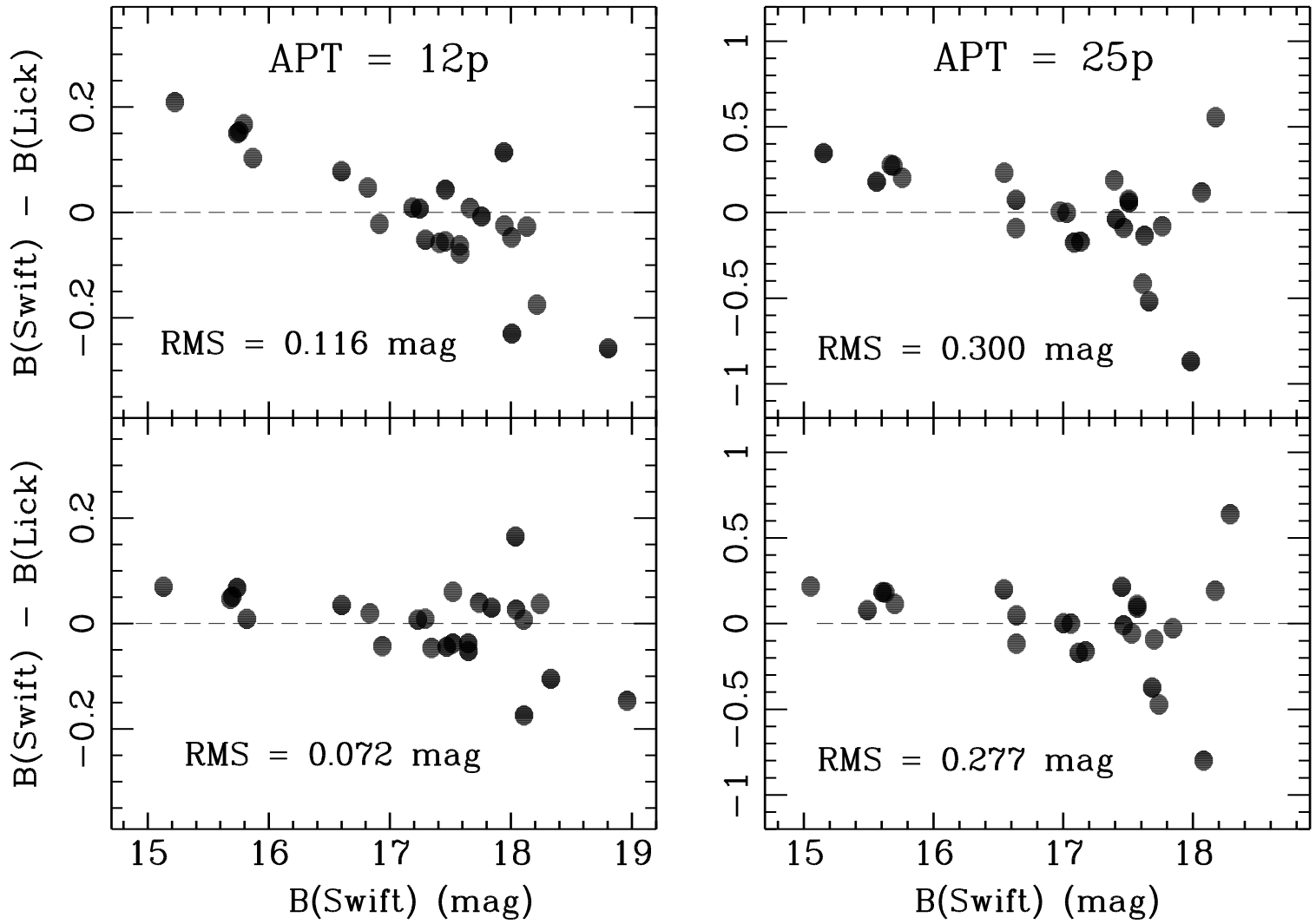


Fig. 11.— Both panels are the same as Figure 8, but for photometry with aperture size = 12 pixels (left), and 25 pixels (right). The correlation between residuals and magnitudes is persistent for both apertures.

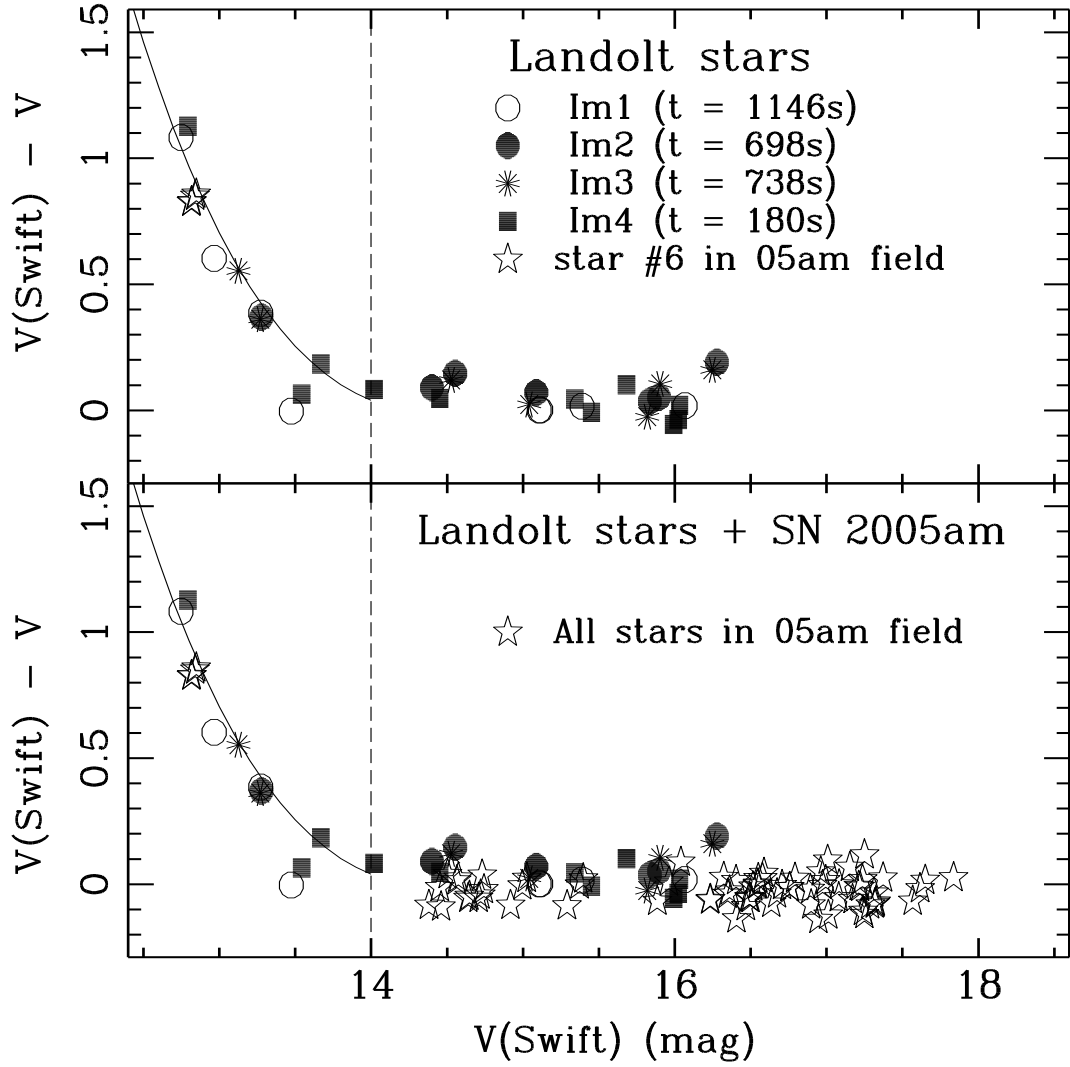


Fig. 12.— Effect of coincidence loss on bright stars in the UVOT photometry. The residual  $V(\text{Swift}) - V$  versus the magnitude  $V(\text{Swift})$  is plotted. Upper panel: the results for the Landolt stars, plus the bright star #6 in the SN 2005am field. Also overplotted is a polynomial fit to the data with  $V(\text{Swift}) < 14$  mag. Lower panel: the same as the upper panel, but with all the measurements for the stars in the SN 2005am field included.

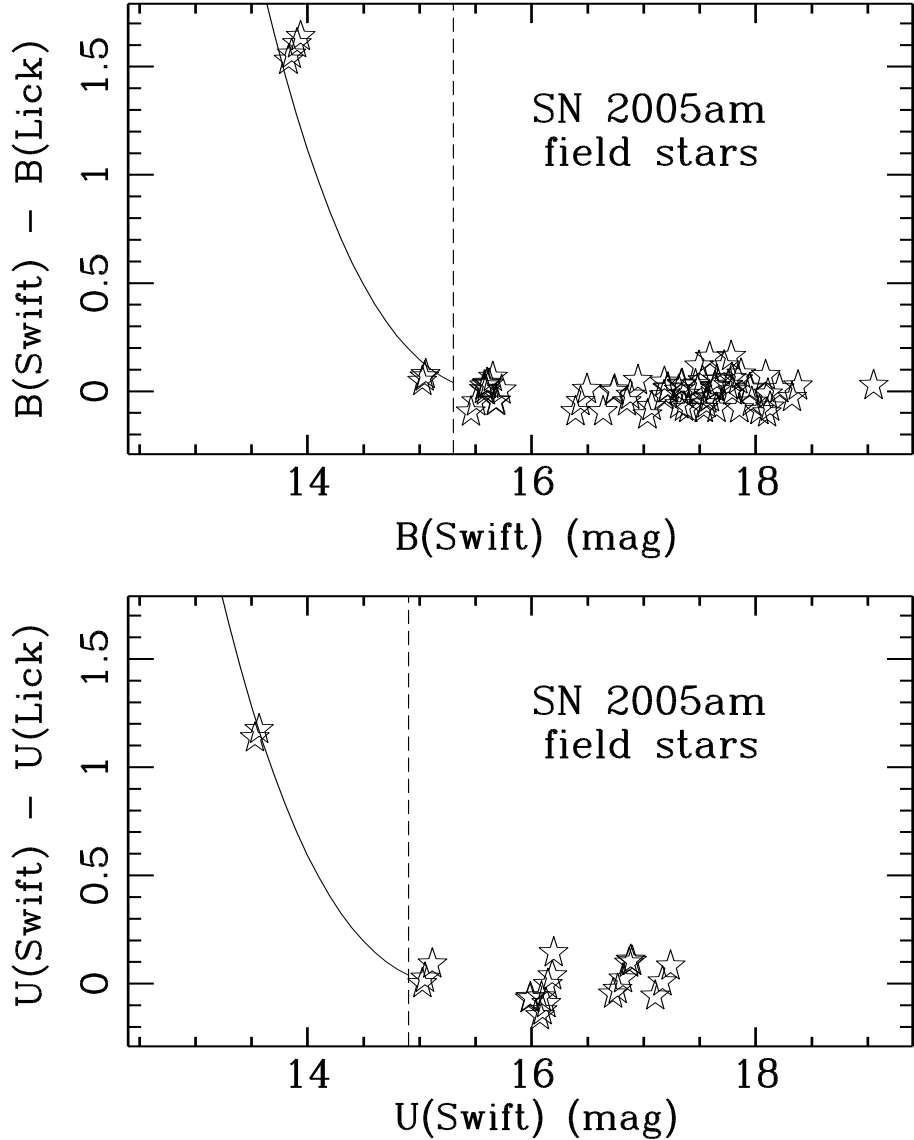


Fig. 13.— Effect of coincidence loss on bright stars in the UVOT photometry. Upper panel: the residual  $B(Swift) - B(Lick)$  versus the magnitude  $B(Swift)$  for all the measurements for the stars in the SN 2005am field, including the bright star #6 (at magnitude around mag 14). Also overplotted is the fit for the Landolt stars as shown in Figure 12, but shifted 1.3 mag in  $B(Swift)$  to match the data by eye. Lower panel: the same as the upper panel, but for  $U(Swift) - U(Lick)$  versus  $U(Swift)$ . The curve is shifted by 0.9 mag in  $U(Swift)$ .

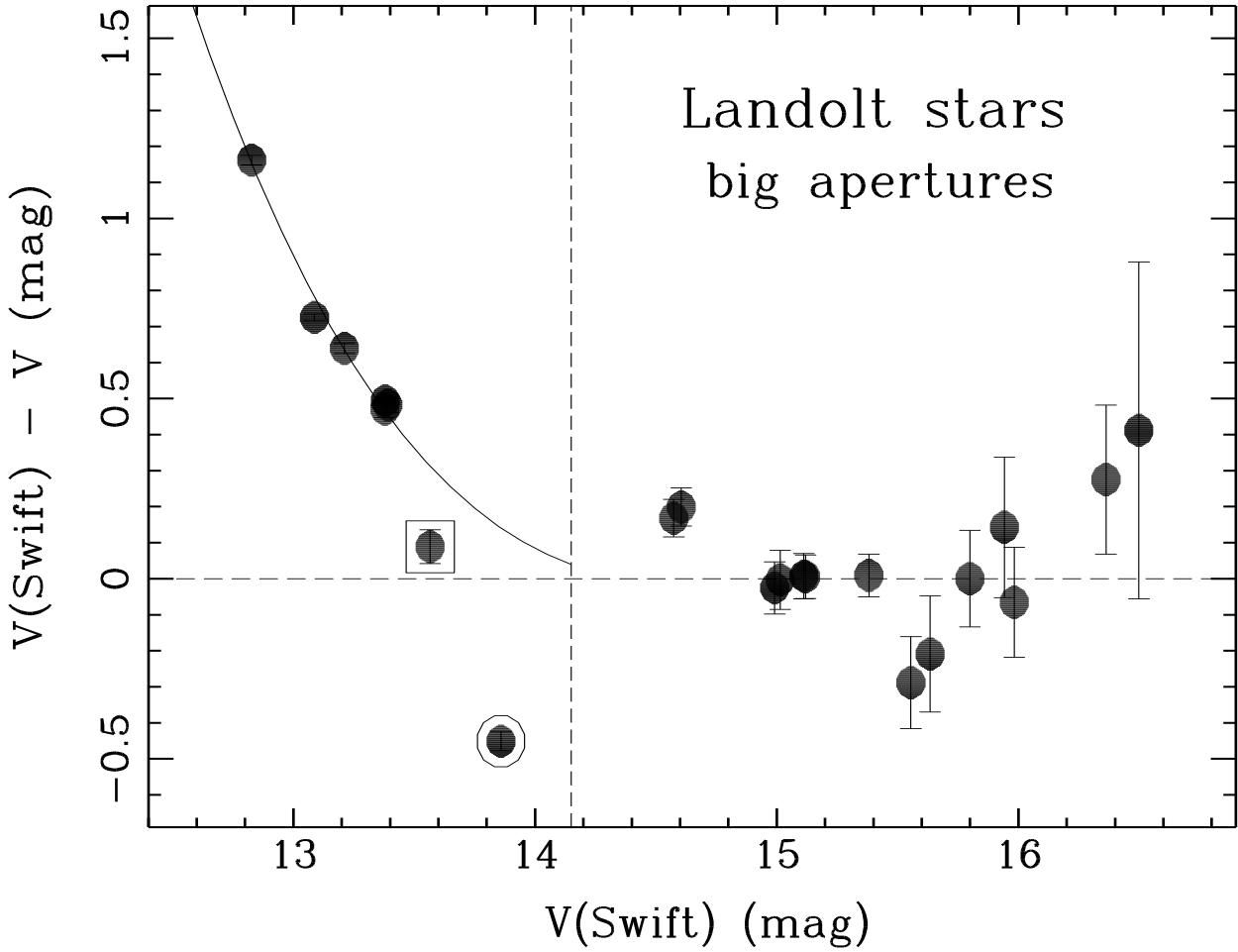


Fig. 14.— Effect of coincidence loss on bright stars in the UVOT photometry. The residual  $V(\text{Swift}) - V$  versus the magnitude  $V(\text{Swift})$  for Landolt stars in im1, im2, and im3. A very big aperture of 60 pixels is used to perform the aperture photometry. The point marked by a circle has another star in the 60-pixel aperture radius, while the point marked by a square is contaminated by a nearby bright star in the photometry aperture. Also overplotted is the solid curve adopted from Figure 12, but shifted by 0.15 mag in  $V(\text{Swift})$ .

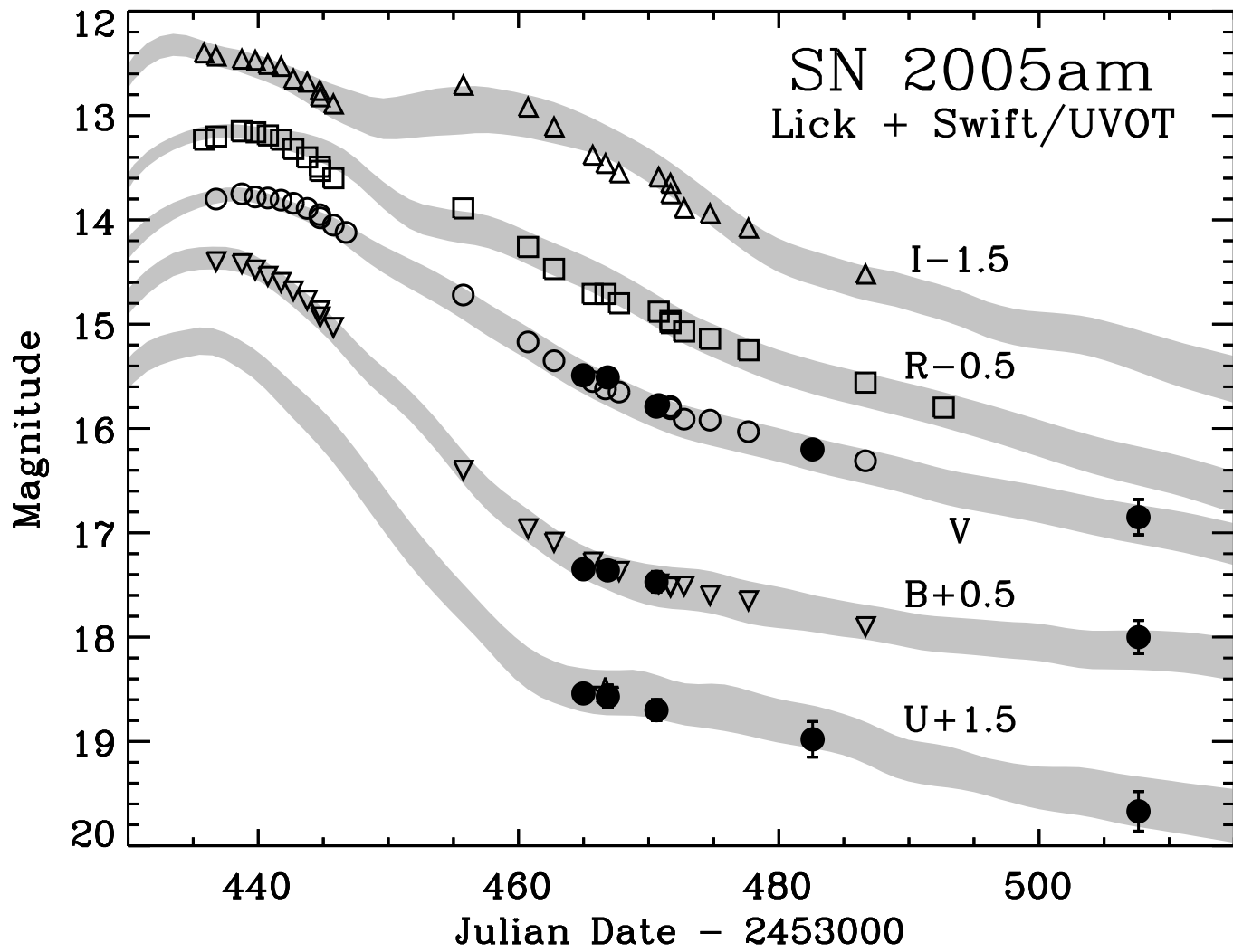


Fig. 15.— The ground-based (open symbols) and the UVOT (solid circles) photometry for SN 2005am. Also overplotted are the MLCS fits.

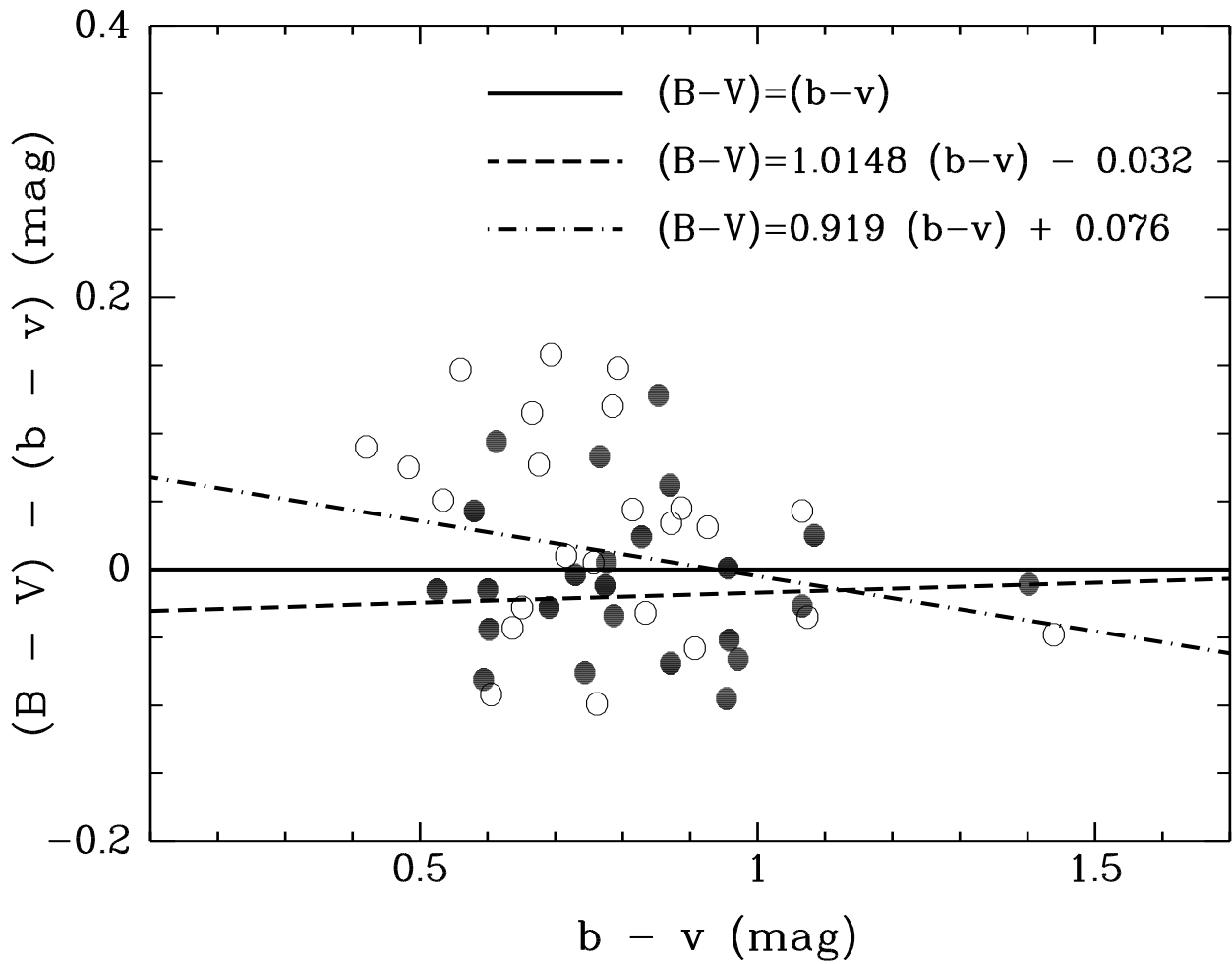


Fig. 16.— The difference between the  $(B - V)$  and  $(b - v)$  color, as a function of  $(b - v)$ . Also overplotted are three fitting functions. The data are consistent with  $(B - V) = (b - v)$ .

This figure "fig01.gif" is available in "gif" format from:

<http://arxiv.org/ps/astro-ph/0505504v1>

This figure "fig03.gif" is available in "gif" format from:

<http://arxiv.org/ps/astro-ph/0505504v1>